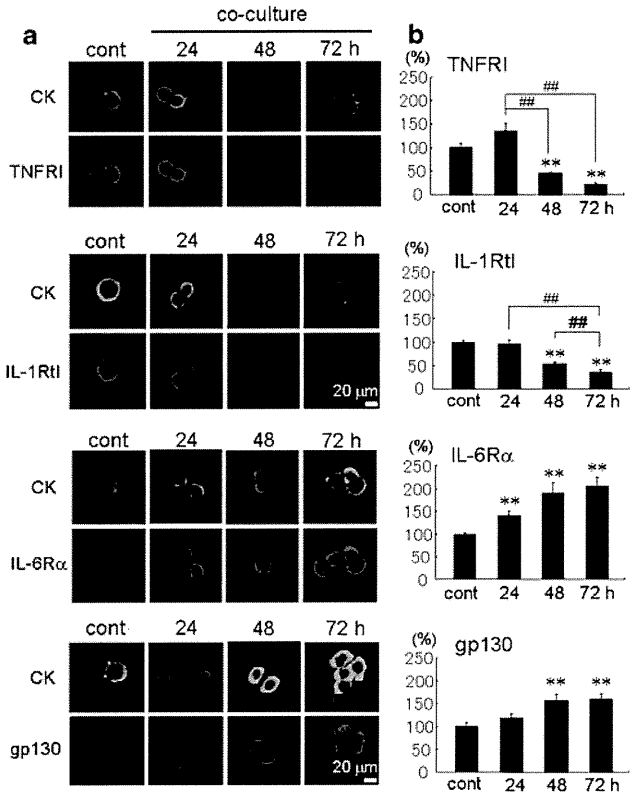

Fig. 6 Time-dependent expression of cytokine receptors on HARA-B cells. **a** Immunostaining of cytokine receptor and receptor subunit (IL-6Rα, gp130, TNFRtI and IL-1RtI) on HARA-B cells with or without co-culture with astrocytes for 24, 48, and 72 h. HARA-B cells were also immunostained with anti-cytokeratin (CK) antibody. **b** Quantification of fluorescent intensity for each receptor or receptor subunit per area of single cell. Data were given as the percentage of intensity in control HARA-B cells without co-culture (100%). Each value represents the mean ± SEM ($n = 8$). ** $P < 0.01$, ## $P < 0.01$

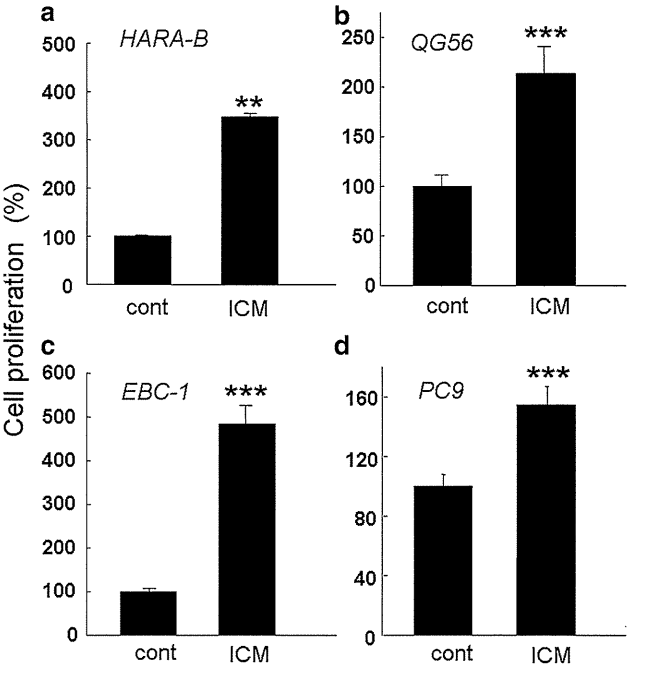

Fig. 7 Increased proliferation of different lung cancer cell lines by astrocytes in vitro. The proliferation of HARA-B cells (**a**), QG56 (**b**), EBC-1 (**c**), PC9 (**d**) were enhanced when they were incubated with insert-culture medium of astrocytes for 72 h. Each value represents the mean ± S.E.M ($n = 4$). *** $P < 0.005$ (significance from control)

microenvironment contains many resident cell types in addition to tumor cells as well as migratory hematopoietic cells.

Though activated astrocytes and soluble factors produced by glial cells in vivo seem to play an important role in the development of brain metastases [5], mechanisms of brain metastases induced by lung cancer cells remained unclear.

In the present study, histological examination revealed that activated astrocytes accumulated around the metastatic foci of human lung cancer-derived cell line, HARA-B cells, in the brain. Similar accumulation of astrocytes around brain metastases was also observed in human brain section from patients with lung cancer metastasis (Fig. 8), as well as in autopsy cases [14]. In our animal models, brain metastases were observed not two but three weeks after intracardiac inoculation of HARA-B cells, mostly in lateral cortex including hippocampus where more GFAP-positive astrocytes were observed even in control condition (data not shown). In later phase of metastases, 4-6 weeks after inoculation, more metastases were observed in whole brain, especially in cerebral cortex. These informations might be useful to understand the process of brain metastasis and its diagnosis.

From our in vitro studies, it was suggested that astrocytes, activated by tumor cells even in the absence of physical contact, promote the proliferation of lung cancer cells by releasing trophic factors. Using one of the lung cancer cell lines, HARA-B cells, IL-1β, TNF-α and IL-6 were identified as astrocyte-oriented factors. It is known that activated astrocytes produce various inflammatory cytokines. IL-1, one of the inflammatory cytokines, has been shown to stimulate the growth of tumor cells in hepatic and/or lung metastases of melanoma tumor cells in vivo [15–17]. Sierra et al. [11] demonstrated that the growth of the breast cancer cell line, which was derived from a brain metastasis, was stimulated by the astrocytes through IL-6, TGF-β and/or IGF-1 in vitro. In brain metastasis of melanoma cells, it was reported that astrocytes produce neurotrophin-regulated heparanase [18, 19]. Recently, it was also reported that epidermal growth factor receptor (EGFR) and membrane type-1 matrix metalloproteinase (MT1-MMP) may be playing an important role in brain metastasis from lung adenocarcinoma and breast cancer [20]. All these results suggest that tumor-promoting

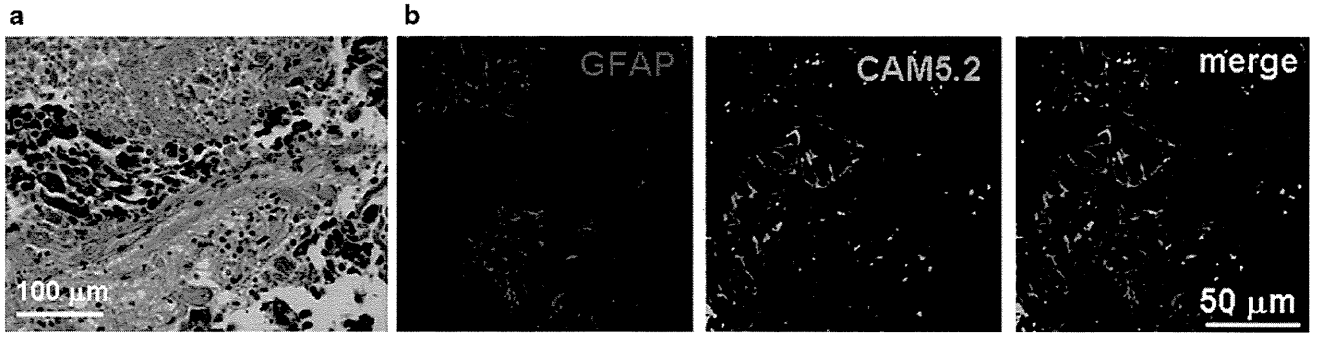

Fig. 8 Astrocytes accumulate around metastasized lung cancer cells in human brain. **a** Hematoxylin and eosin (H & E)-staining of lung cancer cell metastasis (*dark color*) in the human brain section. **b** Immunostaining of astrocytes and tumor cells from human brain section. GFAP-positive astrocytes aggregated around cancer cells (CAM5.2), which looked similar to the brain metastasis of model mice

factors released from astrocytes are different depending on the type of tumor cells and each type of tumor cells may play a different role in the microenvironment of metastatic sites.

So far, a factor produced by HARA-B cells was only a parathyroid hormone-related protein (PTHrP) [21]. However, application of PTHrP(1-34) (10^{-6} M) alone did not stimulate the production of IL-6 in astrocytes (supplementary figure) as was already reported [22]. It was reported that TNF-α stimulated the production of IL-6 in astrocytes and PTHrP acted in an additive fashion with TNF-α to astrocyte-induced expression of IL-6 [22]. In our case, however, PTHrP rather attenuated the effect of TNF-α (100 pg/ml) on astrocytic expression IL-6 (supplementary figure).

In the present study, we found that the production of IL-8, MIF, and SERPINE1 (PAI-1) were markedly increased in the medium of HARA-B cell, with less amount of IL-1ra, IL-2 (Fig. 5a), which increased expression of TNF-α, IL-1β, and IL-6 in astrocytes (Fig. 5b–d). It was recently reported that IL-8, as well as IL-6, were induced in nonsmall-cell lung carcinoma (non-SCLC) cells A549 [23]. In human lung adenocarcinoma cell line CPA-Yang2, which is highly metastasis cell line, quantitative RT–PCR showed that ESM1 (Endothelial cell-specific molecule 1), VEGF-C (Vascular Endothelial Growth Factor C), IL-6, IL-8, AR (androgen receptor) genes were overexpressed [24]. It was also found that IL-8 and matrix metalloproteinase-9 (MMP-9) are important cytokines which are closely related to the growth and metastasis of tumor [25]. Consistently, lung cancer patients had higher levels of serum and bronchoalveolar lavage fluid IL-6 and serum IL-8 compared to controls [26].

As for MIF, it is a multifunctional cytokine or an autocrine- and paracrine-acting cytokine/growth factor, being overexpressed in lung cancer, and therefore one of the biomarkers of non-SCLC [27]. The MIF receptor, CD74, was recently discovered and was found that CD74 and MIF were co-expressed in tumors in close proximity, and that co-expression of the MIF-CD74 pair was associated with both higher levels of tumor-associated angiogenic CXC chemokines and greater vascularity [28]. Importantly, expression level of MIF, together with CD147 proteins, in non-SCLC were related to the metastasis. Survival rate was markedly lower in patients with high expression level of MIF or CD147 [29]. It was also shown that MIF overexpression by adenovirus in human lung adenocarcinoma cells induces a dramatic enhancement of cell migration [30].

Urokinase plasminogen activator (uPA) and its inhibitor PAI-1 stimulate angiogenesis in non-SCLC [31] and a crucial role of PAI-1 in lung cancer invasiveness and influence on prognosis were reported [32–34]. Increased PAI-1 expression and stabilization of PAI-1 mRNA in human lung epithelial and carcinoma cells were regulated by tumor suppressor protein p53 [35]. Taken together, IL-8, MIF, and PAI-1 in lung cancer cells are important not only for invasiveness and prognosis but also as stimulants for astrocytes after brain metastasis.

Stimulated astrocytes by the factors mentioned above release IL-1β, TNF-α and IL-6. In our present study, expression of their receptors on HARA-B cells was confirmed immunocytochemically. Interestingly, the time-dependent change in the expression of receptors for each cytokine seemed different in vitro. IL-6 receptor and its subunit, gp130, were up-regulated with time, while expression of receptors for IL-1β and TNF-α were down-regulated. It was reported that leukocytes rapidly lose their surface receptors for TNF and IL-1 upon exposure to various stimuli in vitro and in fact lipopolisaccharide (LPS) induced down-regulation of monocyte and granulocyte receptors for TNF and IL-1 in humans in vivo [36]. In parallel, the release of IL-6 looked to be delayed compared to that of IL-1β and TNF-α (Fig. 3b, c, d). Taking account

of these evidences, IL-1β and TNF-α might play an important role at the beginning, then IL-6 and its receptors would become more important functionally when brain metastases take place during long period. This might be the reason why the effects of neutralizing antibodies against IL-1β and TNF-α looked apparently robust when they were added during the first 24–72 h of co-culture. Considering the long-lasting effect of IL-6, blocking IL-6 may be useful not only for autoimmune and chronic inflammatory diseases [37] but also for brain metastasis. In vivo analyses on the effects of these cytokine blockages are now under investigation.

The role of activated microglia also needs to be investigated. It was reported that differential reactions of microglia to brain metastasis of lung cancer [38], showing an obvious increase in the number of microglia around metastatic lung cancer mass in the brain. However, only a few microglia expressed inducible nitric oxide synthase (iNOS) and TNF-α in the region where the tumor mass was situated. In vitro study, LPS-activated microglia showed both apoptotic effect and trophic effect, depending on the concentration of supernatant. Since the mechanism would be different between LPS- and metastasis-induced microglial activation, further investigation would be necessary.

In conclusion, the present results showed that the interaction between metastatic tumor cells and activated astrocytes are important in creating a favorable microenvironment for the tumor cells in the brain. They stimulate each other; first lung tumor cells stimulate astrocytes by releasing IL-8, MIF, and PAI-1, then activated astrocytes stimulate the proliferation of tumor cells by releasing cytokines such as TNF-α, IL-1β, and IL-6. These mutual relationships may be important to understand how lung cancer cells metastasize and develop in the brain.

Acknowledgments We thank Prof. D. A. Brown (University College London, UK) for reading the manuscript. This work was supported by Grants-in Aid for Scientific Research of Japan Society for Promotion of Science.

Conflict of interest All authors have no conflict of interest and no financial conflicts.

References

1. Schouten LJ, Rutten J, Huveneers HA, Twijnstra A (2002) Incidence of brain metastases in a cohort of patients with carcinoma of the breast, colon, kidney, and lung and melanoma. Cancer 94:2698–2705
2. Fidler IJ, Yano S, Zhang RD et al (2002) The seed and soil hypothesis: vascularisation and brain metastases. Lancet Oncol 3:53–57
3. Aloisi F, Ria F, Adorini L (2000) Regulation of T-cell responses by CNS antigen-presenting cells: different roles for microglia and astrocytes. Immunol Today 21:141–147
4. Balkwill F, Mantovani A (2001) Inflammation and cancer: back to Virchow? Lancet 357:539–554
5. Fitzgerald DP, Palmieri D, Hua E et al (2008) Reactive glia are recruited by highly proliferative brain metastases of breast cancer and promote tumor cell colonization. Clin Exp Metastasis 25(7):799–810
6. Miller RH, Ffrench-Constant C, Raff MC (1989) The macroglial cells of the rat optic nerve. Annu Rev Neurosci 12:517–534
7. Aloisi F, Care A, Borsellino G et al (1992) Production of hemolymphopoietic cytokines (IL-6, IL-8, colony-stimulating factors) by normal human astrocytes in response to IL-1 beta and tumor necrosis factor-alpha. J Immunol 149:2358–2366
8. Hertz L, McFarlin DE, Waksman BH (1990) Astrocytes: auxiliary cells for immune responses in the central nervous system? Immunol Today 11:265–268
9. Lee SC, Liu W, Dickson DW et al (1993) Cytokine production by human fetal microglia and astrocytes. Differential induction by lipopolysaccharide and IL-1 beta. J Immunol 150:2659–2667
10. Wang FW, Jia DY, Du ZH et al (2009) Roles of activated astrocytes in bone marrow stromal cell proliferation and differentiation. Neuroscience 160(2):319–329
11. Sierra A, Price JE, Garcia-Ramirez M et al (1997) Astrocyte-derived cytokines contribute to the metastatic brain specificity of breast cancer cells. Lab Invest 77:357–368
12. Iguchi H, Tanaka S, Ozawa Y et al (1996) An experimental model of bone metastasis by human lung cancer cells: the role of parathyroid hormone-related protein in bone metastasis. Cancer Res 56:4040–4043
13. Lyons S, Kettenmann K (1998) Oligodendrocytes and microglia are selectively vulnerable to combined hypoxia and hypoglycemia injury in vitro. J Cereb Blood Flow Metab 18:521–530
14. Zhang M, Olsson Y (1995) Reactions of astrocytes and microglial cells around hematogenous metastases of the human brain. Expression of endothelin-like immunoreactivity in reactive astrocytes and activation of microglial cells. J Neurol Sci 134:26–32
15. Giavazzi R, Garofalo A, Bani MR et al (1990) Interleukin 1-induced augmentation of experimental metastases from a human melanoma in nude mice. Cancer Res 50:4771–4775
16. Vidal-Vanaclocha F, Amezaga C, Asumendi A et al (1994) Interleukin-1 receptor blockade reduces the number and size of murine B16 melanoma hepatic metastases. Cancer Res 54: 2667–2672
17. Vidal-Vanaclocha F, Alvarez A, Asumendi A (1996) Interleukin 1 (IL-1)-dependent melanoma hepatic metastasis in vivo; increased endothelial adherence by IL-1-induced mannose receptors and growth factor production in vitro. J Natl Cancer Inst 88:198–205
18. Marchetti D, Denkins Y, Reiland J et al (2003) Brain-metastatic melanoma: a neurotrophic perspective. Pathol Oncol Res 9(3):147–158
19. Denkins Y, Reiland J, Roy M et al (2004) Brain metastases in melanoma: roles of neurotrophins. Neuro Oncol 6(2):154–165
20. Yoshida S, Takahashi H (2009) Expression of extracellular matrix molecules in brain metastasis. J Surg Oncol 100(1):65–68
21. Iguchi H, Onuma E, Sato K et al (2001) Involvement of parathyroid hormone-related protein in experimental cachexia induced by a human lung cancer-derived cell line established from a bone metastasis specimen. Int J Cancer 94(1):24–27
22. Funk JL, Trout CR, Wei H et al (2001) Parathyroid hormone-related protein (PTHrP) induction in reactive astrocytes following

brain injury: a possible mediator of CNS inflammation. Brain Res 915(2):195–209
23. Bauer M, Gräbsch C, Gminski R et al (2010) Cement-related particles interact with proinflammatory IL-8 chemokine from human primary oropharyngeal mucosa cells and human epithelial lung cancer cell line A549. Environ Toxicol. doi:10.1002/tox.20643
24. Yang S, Su J, Cao J et al (2009) Establishment of a novel Chinese human lung adenocarcinoma cell line CPA-Yang1 which produces highly bone metastases in immunodeficient mice. Zhongguo Fei Ai Za Zhi 12(7):753–759
25. Liu Z, Xu S, Xiao N et al (2010) Overexpression of IL-8 and MMP-9 confer high malignant phenotype in patients with non-small cell lung cancer. Zhongguo Fei Ai Za Zhi 13(8):795–802
26. Crohns M, Saarelainen S, Laine S et al (2010) Cytokines in bronchoalveolar lavage fluid and serum of lung cancer patients during radiotherapy—association of interleukin-8 and VEGF with survival. Cytokine 50(1):30–36
27. Khan N, Cromer CJ, Campa M, Patz EF Jr (2004) Clinical utility of serum amyloid A and macrophage migration inhibitory factor as serum biomarkers for the detection of nonsmall cell lung carcinoma. Cancer 101(2):379–384
28. McClelland M, Zhao L, Carskadon S, Arenberg D (2009) Expression of CD74, the receptor for macrophage migration inhibitory factor, in non-small cell lung cancer. Am J Pathol 174(2):638–646
29. Liu Q, Yang H, Zhang SF (2010) Expression and significance of MIF and CD147 in non-small cell lung cancer. Sichuan Da Xue Xue Bao Yi Xue Ban 41(1):85–90
30. Rendon BE, Roger T, Teneng I et al (2007) Regulation of human lung adenocarcinoma cell migration and invasion by macrophage migration inhibitory factor. J Biol Chem 282(41):29910–29918
31. Offersen BV, Pfeiffer P, Andreasen P, Overgaard J (2007) Urokinase plasminogen activator and plasminogen activator inhibitor type-1 in nonsmall-cell lung cancer: relation to prognosis and angiogenesis. Lung Cancer 56(1):43–50
32. Ramer R, Rohde A, Merkord J et al (2010) Decrease of plasminogen activator inhibitor-1 may contribute to the anti-invasive action of cannabidiol on human lung cancer cells. Pharm Res 27(10):2162–2174
33. Chorostowska-Wynimko J, Kedzior M, Struniawski R et al (2010) Cell phenotype determines PAI-1 antiproliferative effect—suppressed proliferation of the lung cancer but not prostate cancer cells. Pneumonol Alergol Pol 78(4):279–283
34. Di Bernardo MC, Matakidou A, Eisen T, Houlston RS (2009) GELCAPS Consortium. Plasminogen activator inhibitor variants PAI-1 A15T and PAI-2 S413C influence lung cancer prognosis. Lung Cancer 65(2):237–241
35. Shetty S, Shetty P, Idell S et al (2008) Regulation of plasminogen activator inhibitor-1 expression by tumor suppressor protein p53. J Biol Chem 283(28):19570–19580
36. van der Poll T, Coyle SM, Kumar A et al (1997) Down-regulation of surface receptors for TNF and IL-1 on circulating monocytes and granulocytes during human endotoxemia: effect of neutralization of endotoxin-induced TNF activity by infusion of a recombinant dimeric TNF receptor. J Immunol 158(3):1490–1497
37. Mihara M, Ohsugi Y, Kishimoto T (2009) Evidence for the role of Th17 cell inhibition in the prevention of autoimmune diseases by anti-interluekin-6 receptor antibody. Biofactors 35(1):47–51
38. He BP, Wang JJ, Zhang X et al (2006) Differential reactions of microglia to brain metastasis of lung cancer. Mol Med 12(7–8):161–170

nature
cell biology

Ciliary transition zone activation of phosphorylated Tctex-1 controls ciliary resorption, S-phase entry and fate of neural progenitors

Aiqun Li[1], Masaki Saito[1,2,3], Jen-Zen Chuang[1], Yun-Yu Tseng[1], Carlos Dedesma[1], Kazuhito Tomizawa[4], Taku Kaitsuka[4] and Ching-Hwa Sung[1,5,6]

Primary cilia are displayed during the G_0/G_1 phase of many cell types. Cilia are resorbed as cells prepare to re-enter the cell cycle, but the causal and molecular link between these two cellular events remains unclear. We show that Tctex-1 phosphorylated at Thr 94 is recruited to ciliary transition zones before S-phase entry and has a pivotal role in both ciliary disassembly and cell cycle progression. However, the role of Tctex-1 in S-phase entry is dispensable in non-ciliated cells. Exogenously adding a phospho-mimic Tctex-1^{T94E} mutant accelerates cilium disassembly and S-phase entry. These results support a model in which the cilia act as a brake to prevent cell cycle progression. Mechanistic studies show the involvement of actin dynamics in Tctex-1-regulated cilium resorption. Tctex-1 phosphorylated at Thr 94 is also selectively enriched at the ciliary transition zones of cortical neural progenitors, and has a key role in controlling G_1 length, cell cycle entry and fate determination of these cells during corticogenesis.

Primary cilia are microtubule-based, hair-like organelles that extend from the plasma membrane to sense and transduce extracellular signals. Primary cilia are displayed on G_0/G_1 cells, and are resorbed as the cells re-enter the cell cycle[1]. The biological significance of these temporally coupled cellular events and the molecular mechanisms underlying the transition between these processes are poorly understood.

Radial glial cells are ciliated neural progenitors in the developing neocortex[2]. Radial glia preferentially undergo proliferative division to expand the progenitor population during early corticogenesis, whereas later progenitors preferentially undergo neurogenic division (differentiation). Proliferation and differentiation are modes of division that are characterized by short and long G_1 durations, respectively[3]. Shortening G_1 accelerates cell cycle entry and expands the progenitor population[4,5], whereas lengthening G_1 drives cell cycle exit and differentiation into neurons[6]. The mechanisms that drive the molecular switch between self-renewal and neuronal differentiation in neural progenitors of the developing neocortex remain unclear.

Tctex-1 (or DYNLT) was originally described as a light chain subunit of cytoplasmic dynein[7,8]. However, Tctex-1 can be uncoupled from the dynein complex to perform dynein-independent functions[9]. Tctex-1 is selectively enriched in proliferating neural progenitors of both embryonic (this paper) and adult brains[10]. However, its function in these cells is unknown. Here we show that Tctex-1, when phosphorylated at Thr 94 (phospho(T94)Tctex-1), regulates ciliary resorption and S-phase entry. In the developing neocortex, phospho(T94)Tctex-1 has an important role in the cell cycle regulation of radial glia and maintenance of the proliferating progenitor population.

RESULTS

Tctex-1 has a key role in cilia-dependent S-phase entry

We tested the role of Tctex-1 in cell cycle control by performing loss-of-function analysis in diploid human hTERT-RPE-1 (herein RPE-1) cells[11]. Shortly before serum starvation, cells were transfected with a plasmid encoding Tctex-1 short hairpin RNA (shRNA) and green fluorescent protein (GFP; plasmid labelled as Tctex-1-sh), or a plasmid encoding GFP alone (vector; Fig. 1a). Following 48 h serum starvation, cell cycle re-entry was induced by serum addition. As predicted, a significant increase in the levels of Rb phosphorylated at Ser 795, Rb phosphorylated at Ser 807/811 and cdc2 phosphorylated at Tyr 15 were observed in control cells 24 h after serum treatment (Fig. 1b, c). Rb phosphorylation is required for G_0/G_1–S transition[12], whereas cdc2 phosphorylated at Tyr 15 is a G_2 marker. Serum treatment failed to induce both phosphorylated Rb and phosphorylated cdc2 in cells with suppressed Tctex-1 (Fig. 1b, c), indicating that Tctex-1 is required for cell cycle re-entry.

[1]Margaret M. Dyson Vision Research Institute, Department of Ophthalmology, Weill Medical College of Cornell University, 1300 York Avenue, New York, New York 10065, USA. [2]Institute for International Advanced Interdisciplinary Research, Tohoku University International Advanced Research and Education Organization, Tohoku University, Aoba 6-3, Aramaki, Aoba-ku, Sendai 980-8578, Japan. [3]Department of Cellular Signalling, Graduate School of Pharmaceutical Sciences, Tohoku University, Aoba 6-3, Aramaki, Aoba-ku, Sendai 980-8578, Japan. [4]Department of Molecular Physiology, Faculty of Life Sciences, Kumamoto University, 1-1-1 Honjyo, Kumamoto 860-8556, Japan, [5]Department of Cell and Developmental Biology, Weill Medical College of Cornell University, 1300 York Avenue, New York, New York 10065, USA. [6]Correspondence should be addressed to C-H.S. (chsung@mail.med.cornell.edu)

Received 17 September 2010; accepted 27 January 2011; published online 13 March 2010; DOI: 10.1038/ncb2218

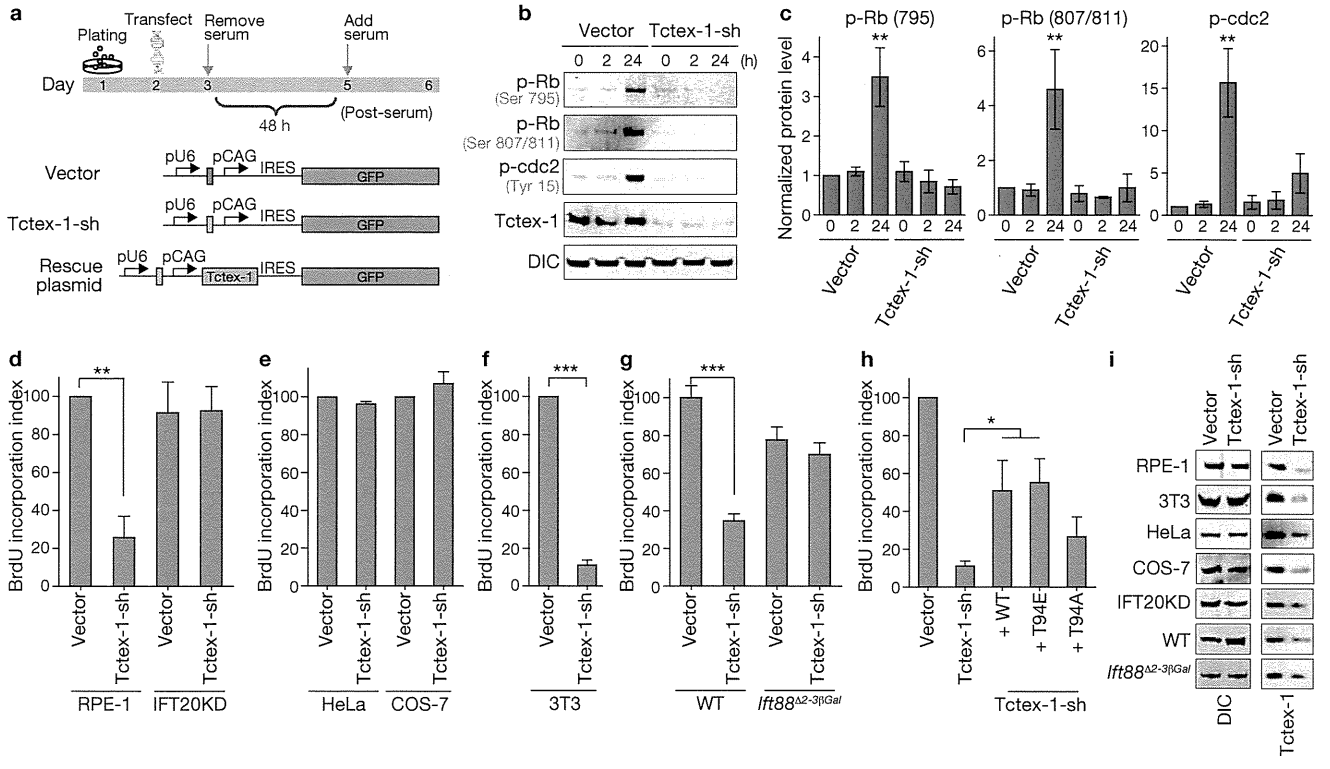

Figure 1 Tctex-1 is involved in cilium-dependent cell cycle re-entry. (**a**) Schematic representations of the timeline of transfection experiments (top) and the plasmids used for transfection (bottom). IRES; internal ribosome entry site. Grey and yellow boxes represent control and *Tctex-1* shRNA sequences, respectively. (**b**) Representative immunoblots of lysates from control- or Tctex-1-sh-transfected RPE-1 cells probed with antibodies against the indicated proteins. Cells were treated as indicated in **a** and the times at which cells were harvested after serum re-addition are shown. p-Rb and p-cdc2, phosphorylated Rb and cdc2, respectively; DIC, dynein intermediate chain. (**c**) Quantification of results from **b**; the signal levels were normalized to the DIC signal. Data are means ± s.e.m.; $n = 3$ experiments, ** $P < 0.01$, *t*-test. (**d**–**h**) BrdU incorporation indices (fraction of BrdU-labelled GFP$^+$ cells) of synchronized RPE-1 or IFT20KD-RPE-1 cells (**d**), HeLa or COS-7 cells (**e**), 3T3 cells (**f**, **h**), and wild-type (WT) or *Ift88* mutant MEF cells (**g**) after serum release. Cells were treated as in **a** and transfected with control vector or Tctex-1-sh plasmid; in **h** cells were additionally transfected with plasmids encoding the indicated Tctex-1 proteins. Incorporation of BrdU in the control cells was taken to be 100%. Data are means ± s.e.m.; $n = 5$, 4, 7, 3 and 7 experiments for figures **d**, **e**, **f**, **g** and **h**, respectively; an average of 400 cells was counted in each experiment; ** $P < 0.01$, *** $P < 0.001$, *t*-test for **d**–**g**; * $P < 0.05$, one-way ANOVA test for **h**. (**i**) Immunoblotting assays of lysates from the indicated cell types transfected with control vector or Tctex-1-sh plasmid. There was a reduction of endogenous Tctex-1 levels in various cell types transfected with Tctex-1-sh plasmid. Uncropped images of blots are shown in Supplementary Fig. S6.

To examine S-phase entry, cells were pulse-labelled with BrdU after serum release, and the fraction of BrdU-labelled GFP$^+$ transfected cells (BrdU incorporation index) was scored (Supplementary Fig. S1a). The BrdU incorporation index of Tctex-1-suppressed cells was significantly lower than that of control cells, indicating that reduced Tctex-1 inhibited S-phase entry (Fig. 1d). S-phase entry was also blocked in unsynchronized cells transfected with either Tctex-1-sh or *Tctex-1* siRNA (short interfering RNA; data not shown). In addition, most control cells were positive for the proliferation marker Ki67, whereas only ~30% of cells transfected with Tctex-1-sh were Ki67 labelled (Supplementary Fig. S1b). These results imply that Tctex-1 suppression induces cell cycle exit (that is, G_0 arrest).

Although a decrease in BrdU incorporation was also seen in 3T3 cells transfected with Tctex-1-sh (Fig. 1f), it was not seen in HeLa and COS-7 cells transfected with Tctex-1-sh (Fig. 1e). As both RPE-1 and 3T3 are ciliated, but HeLa and COS-7 cells are not, we postulated that the role of Tctex-1 in cell cycle progression is cilia-dependent. Two additional 'cilia-free' cell models were employed: a stable RPE-1 cell line in which IFT20 is silenced (that is, IFT20KD-RPE-1; ref. 13), and *Ift88* mutant mouse embryonic fibroblasts (MEF) derived from *Ift88*$^{\Delta 2\text{-}3\beta Gal}$ mice[14,15] (Supplementary Fig. S1c–e). Although Tctex-1 knockdown reduced BrdU incorporation in control RPE cells (Fig. 1d) and wild-type MEF cells (Fig. 1g), it did not affect BrdU incorporation in IFT20KD-RPE-1 (Fig. 1d) and *Ift88*-mutant (Fig. 1g) cells. Similarly, a significantly smaller fraction of Ki67-labelled cells was found in wild-type, but not *Ift88*-mutant MEF cells in which Tctex-1 was suppressed (Supplementary Fig. S1f). Quantification of Tctex-1 level with immunoblots (Fig. 1i) and cell-based immunofluorescence microscopy (Supplementary Fig. S1g, h) showed that the degree of Tctex-1-sh-mediated knockdown was comparable among all cell types tested, confirming that differences were not due to differential gene silencing efficacy. Taken together, these results demonstrate that Tctex-1 has an important role in cilia-dependent S-phase entry.

Transfection of cells with Tctex-1-sh had no effect on the expression levels of several components of the dynein complex, such as dynein intermediate chain (Fig. 1i) and dynein heavy chain[9]. To further test whether the impaired cell cycling mediated by Tctex-1 knockdown was due to its dynein-independent role, we examined whether or not the phosphomimic mutant Tctex-1^{T94E} could rescue the phenotype. Previous studies have shown that Tctex-1^{T94E} fails to be incorporated into the dynein complex, and therefore represents a dynein-free pool of Tctex-1 (ref. 9). A counterpart construct encodes the non-phosphorylatable mutant Tctex-1^{T94A}, which binds dynein[9] and is used here as a control. Thr94 of

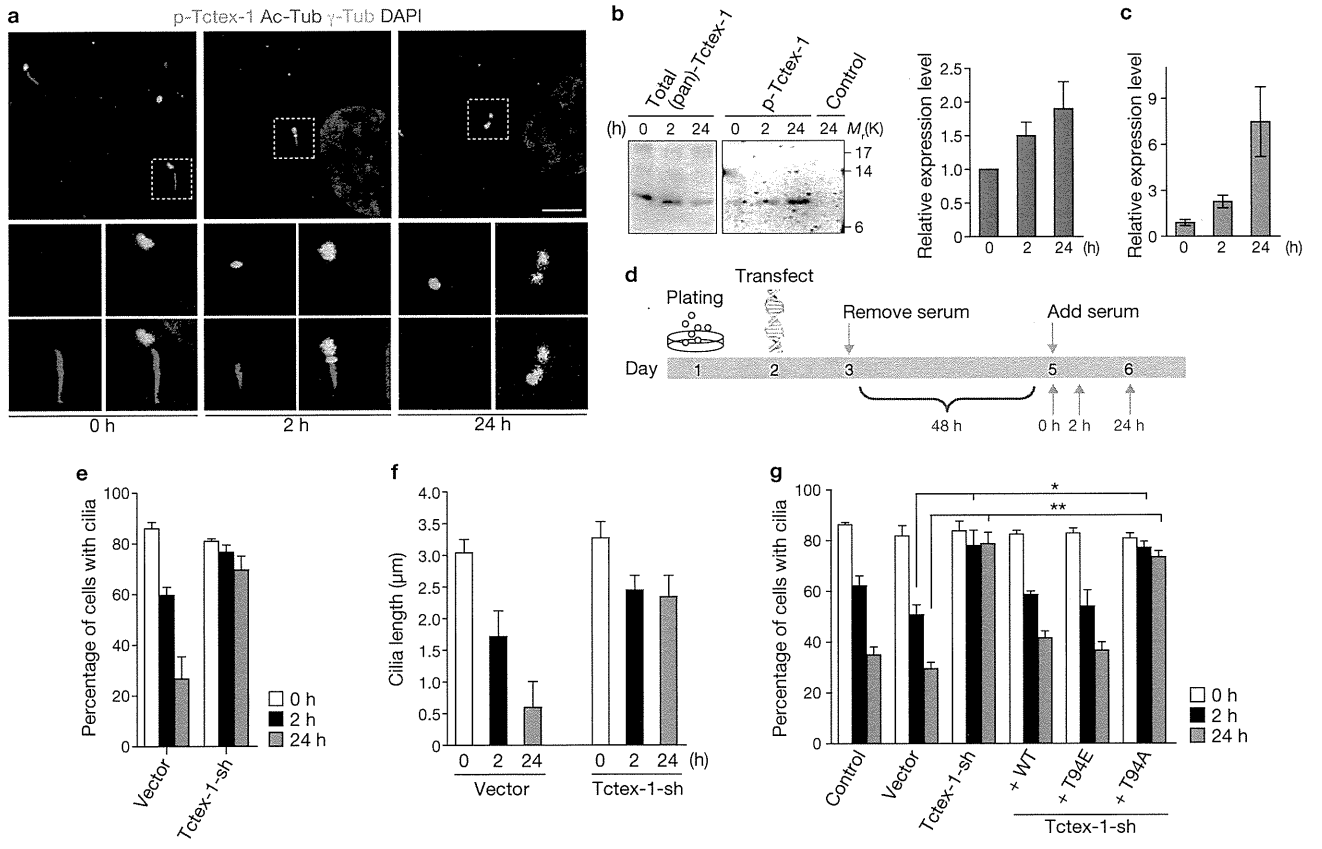

Figure 2 Temporal activation of phospho(T94)Tctex-1 at the transition zone and its function in ciliary disassembly. (**a**) Immunofluorescence microscopy of phosphorylated Tctex-1 (p-Tctex-1; green), acetylated α-tubulin (Ac-Tub; red) and γ-tubulin (γ-Tub; cyan) in quiescent RPE-1 cells or cells treated with serum for 2 h or 24 h. DAPI; nuclei (blue). Insets are higher magnification images of indicated regions. Scale bar, 5 μm. (**b**) Left: representative immunoblots show the levels of (pan)Tctex-1 and phosphorylated Tctex-1 in cells harvested at the indicated times after serum re-addition. To improve the detection of phosphorylated Tctex-1, immunoprecipitation was first carried out using a saturated amount of anti-(pan)Tctex-1, the immunoprecipitates were resolved by electrophoresis and immunoblotted with antibody against phospho(T94)Tctex-1. Anti-HA (haemagglutinin) was used as an immunoprecipitation antibody control. Right: the relative expression level of phospho(T94)Tctex-1 level was normalized to the total amount of immunoprecipitated Tctex-1. (**c**) The relative intensity of phospho(T94)Tctex-1 in immunofluorescence microscopy images of RPE-1 cells at the indicated times after serum re-addition. The ratio of phospho(T94)Tctex-1:γ-tubulin intensity was quantified by MetaMorph software (data are means ± s.e.m.; $n = 3$ experiments). (**d**) Schematic representation of the timeline of cilium disassembly experiments used in **e**–**g**. (**e**) Fraction of transfected RPE-1 cells containing a cilium were scored in cells harvested at the indicated times after serum addition. An average of 500 cells were counted for each experiment (data are means ± s.e.m.; $n = 3$ experiments). (**f**) Quantification of the cilia lengths in transfected 3T3 cells harvested after serum addition (data are means ± s.e.m.; $n = 3$ experiments). (**g**) The fractions of transfected cells containing a cilium. Cells were harvested at indicated times after serum addition and scored and statistically analysed (data are means ± s.e.m.; $n = 5$ experiments; * $P < 0.05$, ** $P < 0.01$; one-way ANOVA). Uncropped images of blots are shown in Supplementary Fig. S6.

Tctex-1 is a conserved residue, and resides within a consensus motif for protein kinase C and integrin-linked kinase (http://www.cbs.dtu.dk/services/NetPhosK/; http://gps.biocuckoo.org/). T94E and T94A variants of Tctex-1 were generated in bovine Tctex-1, which is insensitive to shRNA against mouse Tctex-1, allowing us carry out the rescue experiments in mouse 3T3 cells. Impaired S-phase entry caused by Tctex-1 knockdown can be rescued by the re-introduction of wild-type Tctex-1 and the Tctex-1^{T94E} mutant, but to a much lesser extent by the T94A mutant (Fig. 1h). These results not only suggest that the phenotypes caused by Tctex-1-sh were not an 'off-target' effect, but also that Tctex-1^{T94E} mimicked the functionally active form of Tctex-1.

Temporal and spatial activation of phospho(T94)Tctex-1 at the transition zone is required for ciliary resorption

The kinetics of cilium assembly/disassembly, as well as the temporal relationship between cilium dynamics and cell cycle progression, have been characterized in RPE-1 and 3T3 cells[11,16,17]. In both cell types, serum starvation induces quiescence and cilium formation. The return of serum triggers biphasic ciliary resorption, which peaks at 2 h and 24 h post-serum treatment. The first wave of cilium shortening occurs at mid/late G_1-phase preceding S phase entry, whereas the second wave occurs as cells are preparing to enter the G_2/M phase [16]. Immunolabelling using an antibody specifically recognizing phospho(T94)Tctex-1 showed that phospho(T94)Tctex-1 was rarely seen in quiescent cells (0 h), whereas prominent phospho(T94)Tctex-1 signals were consistently detected at the ciliary base immediately adjacent to the shortened cilia in cells treated with serum for 2 h (Fig. 2a). Phospho(T94)Tctex-1 was specifically distributed to the transition zone between the γ-tubulin-labelled basal bodies and acetylated α-tubulin-labelled cilia. Consistent with the cilia loss and cell cycle re-entry in cells after 24 h serum treatment, phospho(T94)Tctex-1 signals were found on centrosomes in interphase cells (Fig. 2a) and mitotic poles in dividing cells (Supplementary

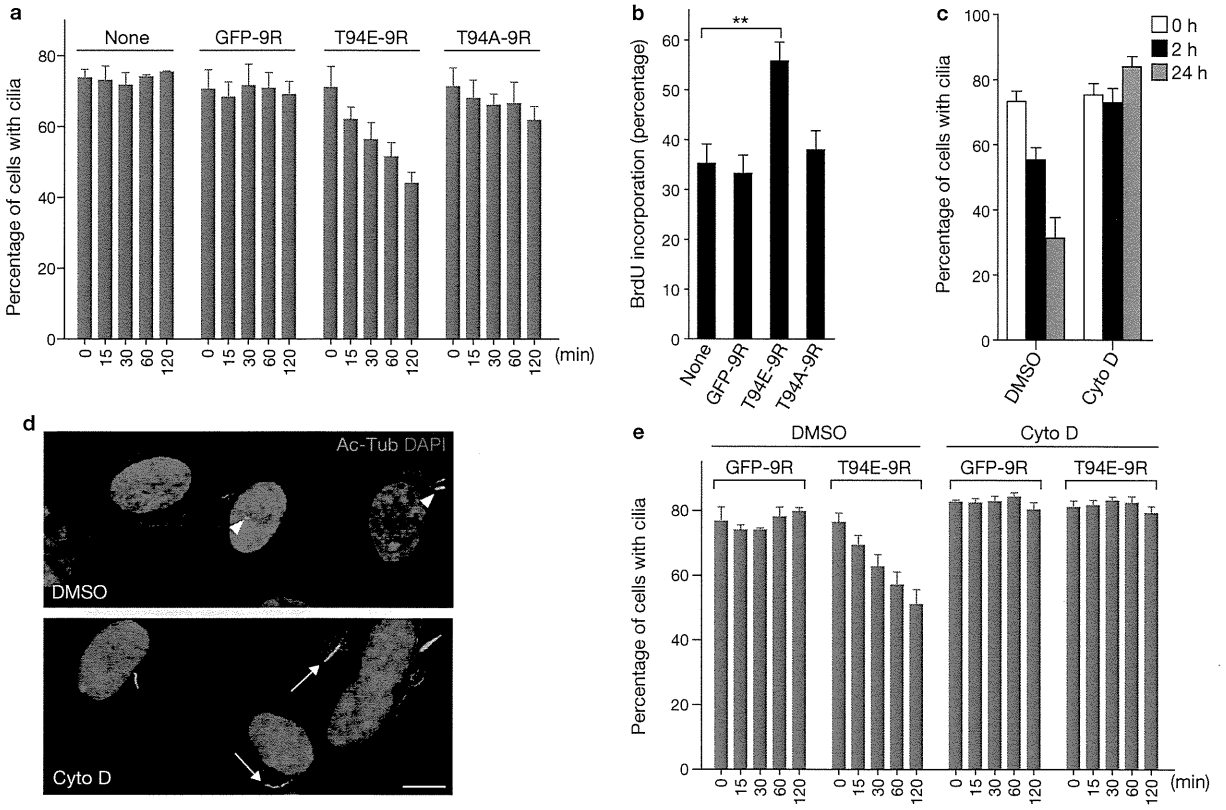

Figure 3 Phospho(T94)Tctex-1 and actin dynamics participate in ciliary resorption. (**a**) Fractions of cells displaying cilia. RPE-1 cells were serum starved and left untreated (none) or treated with GFP-9R, Tctex-1^{T94E}-9R or Tctex-1^{T94A}-9R peptides, and harvested at indicated times after the treatments. Data are means ± s.e.m.; $n = 4$ experiments, except untreated control, where $n = 3$ experiments. (**b**) Cells in serum-free medium were treated with the indicated peptides followed by incubation with BrdU for 16 h. Fractions of BrdU-labelled cells are shown (data are means ± s.e.m.; $n = 7$ experiments; ** $P < 0.01$; one-way ANOVA). (**c**) Cells were treated with DMSO (as a control) or Cyto D (0.5 μM) after serum addition and the fraction of ciliated cells was quantified (data are means ± s.e.m.; $n = 3$ experiments). (**d**) Representative image of cilia displayed in control cells versus Cyto D-treated cells 24 h after serum addition. Arrowheads and arrows indicate shortened and long cilia in the DMSO- and Cyto D-treated cells, respectively. Scale bar, 5 μm. (**e**) Fractions of cells that had cilia after the addition of GFP-9R or Tctex-1^{T94E}-9R for indicated time in the presence of DMSO ($n = 3$ experiments) or Cyto D ($n = 5$ experiments). Data are means ± s.e.m.

Information Fig. S2a). Quantitative immunoblotting and immunofluorescence microscopy assays showed that the level of phospho(T94) Tctex-1 gradually increases with serum re-addition (Fig. 2b, c).

Pre-absorption of the antibody with the antigen peptide, but not the control peptide (corresponding to the antigen except lacking the phospho(T94) modification), effectively removed the phospho(T94) Tctex-1 signals (Supplementary Fig. S2b). The signal from phospho(T94) Tctex-1 in immunofluorescence microscopy images was greatly reduced in the RPE-1 cells transfected with Tctex-1-sh (Supplementary Fig. S2c). Furthermore, phospho-Tctex-1 signal on immunoblots was sensitive to the treatment of alkaline phosphates (Supplementary Fig. S2d). These results confirm the specificity of phospho(T94)Tctex-1 immunolabelling.

The appearance of phospho(T94)Tctex-1 at the ciliary base shortly preceding the disassembly of cilia indicates its functional involvement in this cellular event. To directly test the role of Tctex-1 in ciliary disassembly, serum-starved cells transfected with Tctex-1-sh were harvested at 0 h, 2 h and 24 h after serum re-addition (Fig. 2d). The fraction of GFP$^+$ cells displaying a cilium and the length of the cilia in transfected cells were scored. In RPE-1 (Fig. 2e), 3T3 (Fig. 2f, g), and MEF (Supplementary Fig. S2e) cells, controls and Tctex-1-suppressed cells had similar abilities to form cilia after serum starvation. The lengths of their cilia were also similar (Fig. 2f). However, serum-induced cilium disassembly was significantly blocked by Tctex-1 suppression, suggesting that Tctex-1 is not required for ciliogenesis, but is critical for cilium disassembly. Furthermore, co-transfection of Flag-tagged wild-type Tctex-1 or Tctex-1^{T94E}, but not Tctex-1^{T94A}, with Tctex-1-sh effectively reversed the inhibition of cilium disassembly caused by Tctex-1 silencing (Fig. 2g).

To further investigate the causal relationship between ciliary disassembly and S-phase entry, we investigated whether or not exogenously added Tctex-1^{T94E} can trigger rapid cilium disassembly of RPE-1 cells, and thus accelerate their S-phase entry. We employed a high-efficiency protein transduction system[18] to deliver Tctex-1 peptides into RPE-1 cells with pre-formed cilia. Purified recombinant Tctex-1 (or GFP) containing a nine-arginine sequence (9R) entered cells effectively, as confirmed by both immunoblotting and immunostaining assays (Supplementary Fig. S2f, g). The addition of control peptides GFP-9R and Tctex-1^{T94A}-9R had no effect on cilia disassembly (Fig. 3a). In contrast, cells treated with Tctex-1^{T94E}-9R underwent significantly faster cilium resorption even when cultured in the absence of serum (Fig. 3a). Cells treated with Tctex-1^{T94E}-9R, but not control peptides, also exhibited significantly higher BrdU incorporation (Fig. 3b).

Phospho(T94)Tctex-1 has a reported ability to modulate actin dynamics[9]. To investigate the role of actin in cilium resorption, we

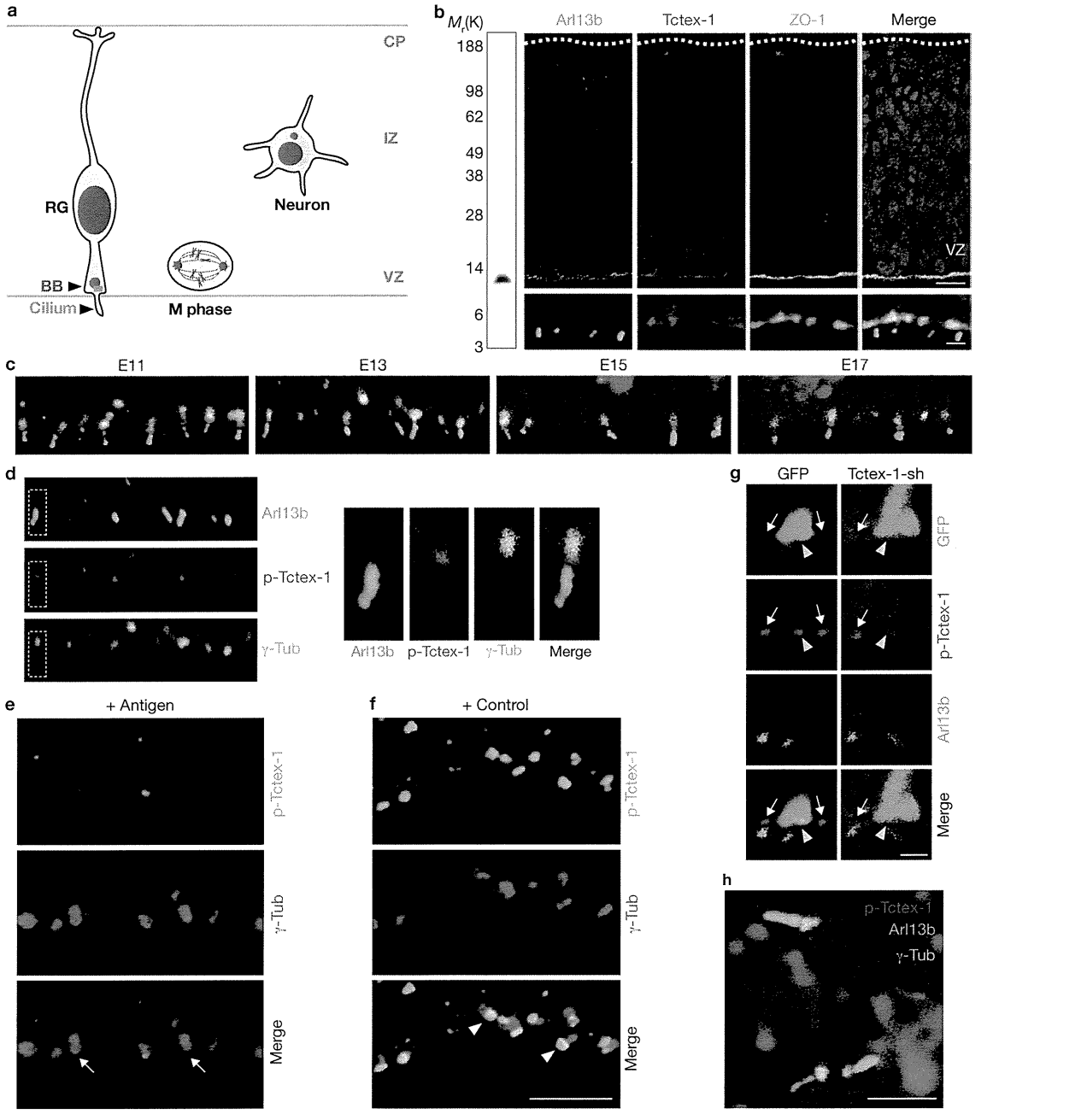

Figure 4 Phospho(T94)Tctex-1 is expressed at the transition zone of radial glia in the developing neocortex. (**a**) Schematic representation of the radially elongated radial glia with their endfeet contacting both the ventricular and pial surfaces. The primary cilium, anchored on a basal body (BB), extends into ventricular spaces. Mitosis (M phase) typically occurs at the ventricular surfaces. Cells leave the cell cycle, migrate away from the ventricular zone (VZ), form multipolar post-mitotic neurons, and pause their migration in the intermediate zone (IZ) before reaching their cortical location. CP; cortical plate. (**b**) Left: anti-Tctex-1 mouse antibody recognized a single band of M_r ~12K on an immunoblot containing embryonic mouse brain lysates. Right: E13 mouse cortical slices were co-labelled for cilium marker Arl13b (ref. 42; green), Tctex-1 (red), and cell–cell junction marker ZO-1 (cy5). Dotted lines represent the ventral borders. Bottom images are enlarged views of the labelling of the ventricle surface. Scale bars, 20 μm (top); 2 μm (bottom). (**c**) Ventricle surfaces of E11–E17 mouse neocortical slices were triple-labelled for Arl13b (green), phospho(T94)Tctex-1 (red) and γ-tubulin (cyan). (**d**) Higher-magnification images (right) of indicated area from an image of an E13 ventricle surface (left; as shown in **c**). Phospho(T94)Tctex-1 (red) was specifically located in the transition zone between the Arl13b-labelled cilia (green) and the γ-tubulin-labelled basal bodies (cyan) of the radial glia. (**e**, **f**) Confocal microscopy images of the ventricular zone from mice brains, double labelled with antibodies against γ-tubulin and phospho(T94) Tctex-1 pre-absorbed with phosphopeptides corresponding to the antigen (**e**) or control peptides (**f**). Arrows in **e** indicate the γ-tubulin-labelled basal bodies and centrosomes, which lacked the phospho(T94)Tctex-1 signal. Arrowheads indicate the phospho(T94)Tctex-1 signals that remained at the ciliary base. Scale bar, 5 μm. (**g**) Co-labelling of phospho(T94) Tctex-1 and Arl13b in mouse cortical slices 24 h after transfection. Note that cells transfected with GFP control plasmid (left, green arrowhead) and neighbouring non-transfected cells (arrows) displayed similar levels of phospho(T94)Tctex-1 at the endfeet. However, cells transfected with Tctex-1-sh (right, green arrowhead) had reduced immunolabelling of phospho(T94)Tctex-1 (arrow indicates neighbouring non-transfected cell). Scale bar, 2 μm. (**h**) Post-mitotic mouse neurons located in the intermediate zone region had no detectable phospho(T94)Tctex-1 (red) between the Arl13-labelled cilia (green) and γ-tubulin-labelled basal bodies (cyan). Scale bar, 5 μm.

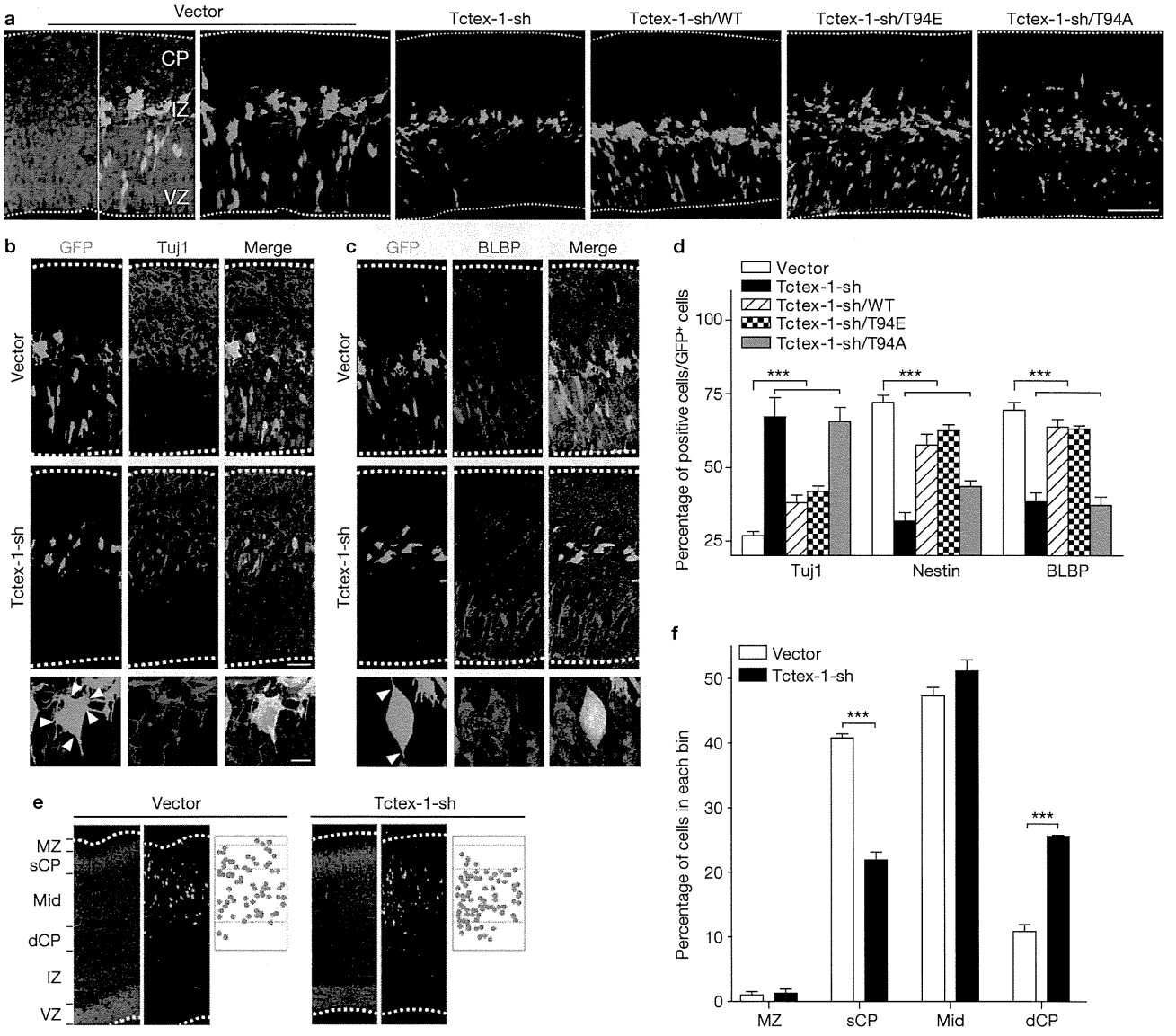

Figure 5 Suppression of Tctex-1 in radial glia induced premature neuronal differentiation. (**a**) Mouse cortical slices harvested 40 h after electroporation with the indicated plasmids. GFP was detected by direct green immunofluoresence microscopy. DAPI; blue. The dashed lines depict the borders of the cortexes. The intermediate zone (IZ) is defined by the presence of tangentially oriented cells. (**b**, **c**) Representative images showing the labelling of Tuj1 (**b**) and brain lipid-binding protein (BLBP) (**c**) of vector- and Tctex-1-sh-transfected mouse brain slices. Bottom; higher-magnification images of cells transfected with Tctex-1-sh. Arrowheads point to the sites where the cell processes project from the cell bodies. (**d**) Percentage of total transfected GFP$^+$ cells that were Tuj1$^+$, Nestin$^+$ or BLBP$^+$, quantified from an experiment performed as in **c**. Data are means ± s.e.m.; $n = 4$ experiments, except BLBP staining, where $n = 5$ experiments; an average of 600 cells were counted in each experiment; *** $P < 0.001$, one-way ANOVA. (**e**) Representative images depicting the cortical distribution of GFP cells in brains from mice at E18.5 (that is, 5-days post electroporation). Right; plots of GFP$^+$ cell distribution. Top to bottom; the marginal zone (MZ), superficial (sCP), mid-, and deeper cortical plate (dCP) bins were defined as previously described[43] and are as indicated on the images. (**f**) Quantification of the cortical location of transfected cells from experiment performed as in **e** (data are means ± s.e.m.; $n = 3$ experiments; *** $P < 0.001$, *t*-test).

treated quiescent RPE-1 cells with an actin polymerization inhibitor, cytochalasin D (Cyto D), 2 h before serum addition. Cyto D treatment effectively blocked serum-mediated cilium disassembly (Fig. 3c, d). Furthermore, treatment with Cyto D inhibited Tctex-1^{T94E}-peptide-mediated acceleration of ciliary resorption (Fig. 3e). These results imply that phospho(T94)Tctex-1 modulates cilium disassembly through a process involving actin polymerization.

Previous studies have shown that blocking the activation of histone/tubulin deacetylase-6 (HDAC6) mediated by Aurora A kinase (AurA) phosphorylation suppresses cilium resorption in RPE-1 cells[11]. We tested whether AurA- or HDAC6-depleted cells also exhibit impaired S-phase entry. Our results showed that suppression of both AurA and HDAC6 through shRNA or siRNA transfection were able to inhibit both ciliary resorption and BrdU incorporation (Supplementary Fig. S3a-c).

Phospho(T94)Tctex-1 is expressed in the ciliary transition zone of radial glia in the developing neocortex

The developing neocortex is an ideal model system for studying the physiological relevance of phospho(T94)Tctex-1 *in vivo* because the cortical progenitor radial glia also display primary cilia (Fig. 4a), and

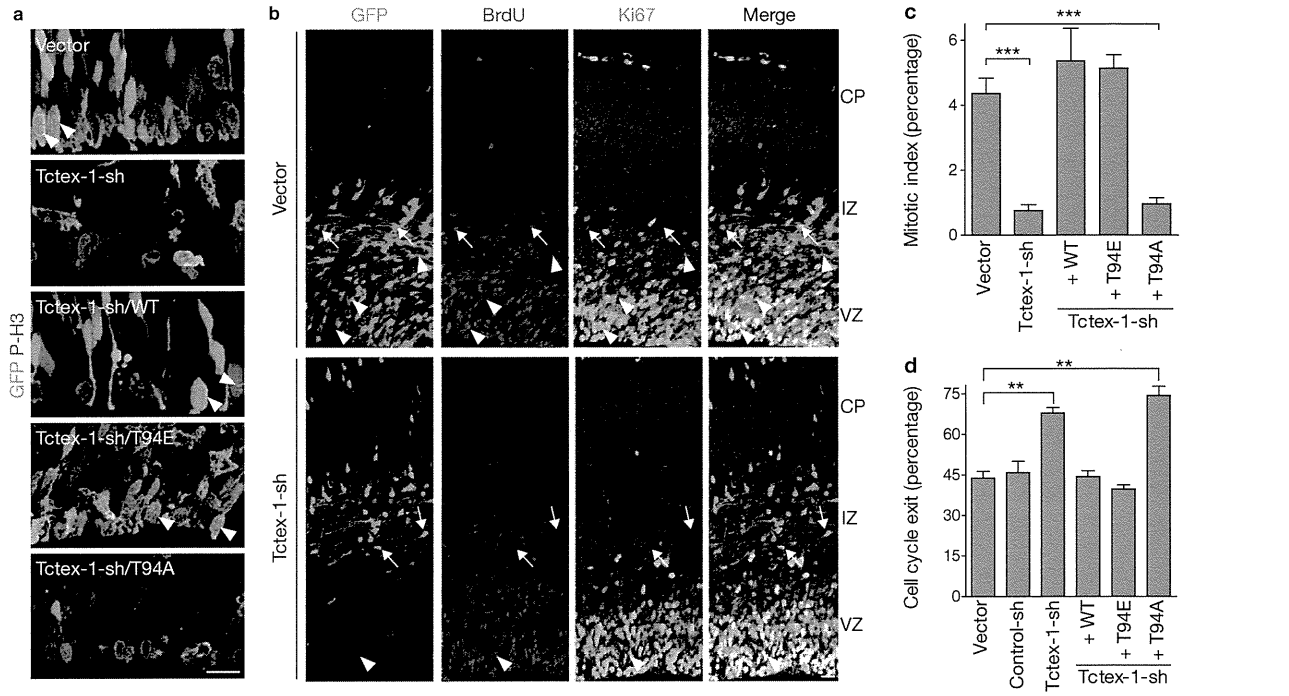

Figure 6 Phosphorylated Tctex-1 is required for cell cycling of radial glia. (**a**) Representative images of the ventricular zone of brains from mice transfected as indicated. Samples were immunolabelled with P-H3. Arrowheads indicate cells that were positive for both GFP and P-H3. (**b**) Representative confocal microscopy images of transfected mouse cortical slices subjected to cell cycle exit analysis. Left, GFP$^+$ cells (green); middle, cells 24 h after BrdU treatment (red) and right, stained with antibodies against Ki67 (cyan). Arrows point to the cells that were positive for GFP and BrdU, but negative for Ki67. Arrowheads point to the cells that were positive for GFP, BrdU and Ki67. (**c**) Fractions of GFP$^+$ and P-H3$^+$ cells out of total GFP$^+$ cells (the mitotic index). Data are means ± s.e.m.; $n = 3$, 6, 3, 5 and 6 experiments for vector, Tctex-sh, Tctex-1-sh/WT, Tctex-1-sh/T94E and Tctex-1-sh/T94A, respectively; *** $P < 0.001$, one-way ANOVA. (**d**) Fractions of GFP$^+$, BrdU$^+$, Ki67$^-$ cells out of total GFP$^+$, BrdU$^+$cells (or cell cycle exit index). Data are means ± s.e.m.; $n = 3$ experiments; total of 100 cells were scored; ** $P < 0.01$, one-way ANOVA.

the relationship between the cell cycle regulation and the fate control of radial glia has already been established[19,20].

Staining embryonic day (E) 11–E17 mouse embryonic cortices with anti-(pan)Tctex-1 antibody showed that Tctex-1 was specifically concentrated at the apical endfeet of radial glia, from which Arl13b-labelled cilia project into the ventricles (Fig. 4b and Supplementary Fig. S4a). However, phospho(T94)Tctex-1 appeared as prominent punctae lining the ventricular surfaces. Co-localization studies confirmed that phospho(T94) Tctex-1 specifically resides in the transition zone between the γ-tubulin-labelled basal bodies and the primary cilia (Fig. 4c, d). The transition zone-labelling of phospho(T94)Tctex-1 was universal in all radial glia regardless of developmental stage, and despite the fact that there were fewer radial glia in later stages of neurogenesis (that is, E17; Fig. 4c). Preabsorption with the antigen, but not control peptide, effectively removed the phospho(T94)Tctex-1 signals (Fig. 4e, f). Phospho(T94) Tctex-1 labelling was also greatly reduced in radial glia transfected with Tctex-1-sh (Fig. 4g). In marked contrast, no phospho(T94)Tctex-1 signal was detected at the bases of primary cilia in the post-mitotic neurons located at the intermediate zone or cortical plate (Fig. 4h), indicating that phospho(T94)Tctex-1 is present in G_1, but not G_0 cells.

Tctex-1 knockdown triggers premature neuronal differentiation at the expense of the neural progenitor pool

The similar transition zone location of phospho(T94)Tctex-1 in radial glia and cultured ciliated cells prompted us to reason that this molecule may also regulate the cell cycling of Radial glia during corticogenesis. If this were the case, the depletion of Tctex-1 would drive radial glia to exit the cell cycle and differentiate into neurons. Post-mitotic neurons typically migrate away from the ventricular zone where the cell division takes place, halt temporarily at the intermediate zone (Fig. 4a), and are eventually incorporated into laminated cortical plates according to their birthdates[21]. We predicted that excess phospho(T94)Tctex-1 would shorten the G_1 phase, accelerate S-phase entry and expand the progenitor population.

To test our model, we employed *in utero* electroporation (IUE), an efficient gene delivery method for radial glia to perform loss-of-function and gain-of-function analyses. To test the first part of our hypothesis, Tctex-1-sh plasmid was transfected into an E13.5 mouse neocortex. Immunolabelling of cells dissociated from brains harvested as early as 24 h and as late as 5 days after IUE verified the specific knockdown of endogenous Tctex-1 in cells transfected with Tctex-1-sh, but not in cells transfected with control plasmid, (Supplementary Fig. S4b). We subsequently conducted phenotypic characterization of cells transfected with Tctex-1-sh *in situ*. Several lines of evidence suggested that Tctex-1 silencing in radial glia caused their premature neuronal differentiation. First, in cortical slices harvested 40 h after electroporation, cells transfected with control and Tctex-1-sh plasmids displayed strikingly different distribution patterns. Cells transfected with either vector alone (Fig. 5a) or control shRNA plasmid (Supplementary Fig. S4c) were distributed throughout the area between the ventricular zone, subventricular zone and intermediate zone. The large majority of these cells had bipolar shapes and expressed radial glia markers Nestin and brain lipid-binding

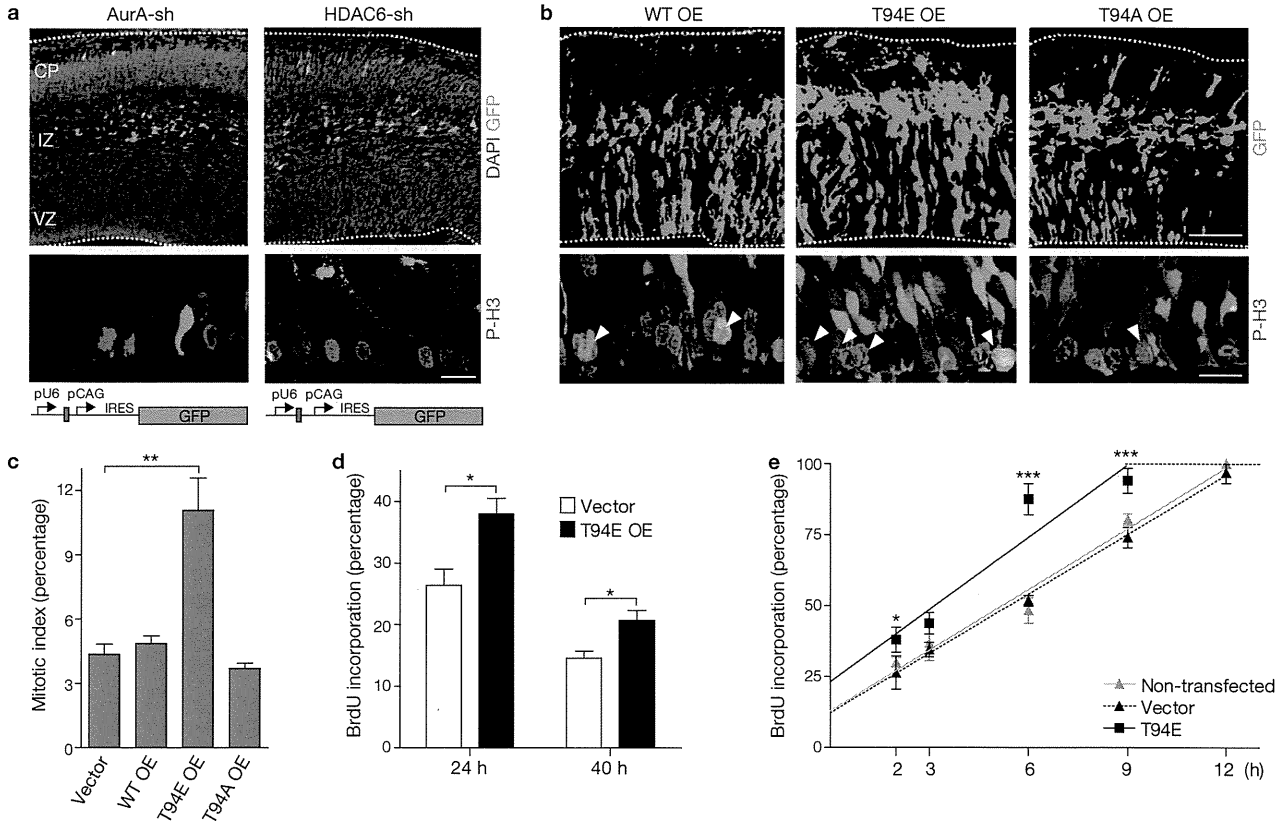

Figure 7 Phenotypic characterization of the developing neocortex of AurA and HDAC6 loss-of-function mutants, and Tctex-1 gain-of-function mutants. **(a)** Mouse cortical slices transfected with AurA-sh or HDAC6-sh plasmid and immunolabelled with P-H3 (red; middle panel). DAPI; blue. Bottom; schematic representation of the respective plasmids. Purple boxes indicate the shRNA-targeting sequences. **(b)** Cortical slices overexpressing the indicated Tctex-1 variants. Arrowheads point to P-H3-labelled, mitotic GFP$^+$ cells at the ventricular zone. Scale bars, 100 μm (top), 20 μm (bottom). **(c)** Mitotic indices of GFP$^+$ cells transfected with plasmids expressing the indicated Tctex-1 variants and GFP. Data are means ± s.e.m.; $n = 3$ experiments; total 1,200 cells were scored; ** $P < 0.01$, one-way ANOVA. **(d)** The fractions of transfected mouse brains with BrdU incorporation (2 h incubation) that were GFP$^+$ cells out of total GFP$^+$ cells, 24 h and 40 h post-electroporation (data are means ± s.e.m.; $n = 4$ experiments; total 700 cells were scored; * $P < 0.05$, *t*-test). **(e)** Cumulative BrdU labelling curves of non-transfected cells and cells transfected with vector alone or Tctex-1^{T94E}/GFP. Data are means ± s.e.m.; $n = 3$ experiments; * $P < 0.05$, *** $P < 0.001$, one-way ANOVA. OE; overexpression.

protein (Fig. 5c, d), and a much smaller fraction of them displayed post-mitotic neuronal marker Tuj1 (Fig. 5b, d). GFP$^+$ control cells localized to the subventricular zone also displayed intermediate progenitor marker Tbr2 (Supplementary Fig. S4d). In contrast, Tctex-1-silenced GFP$^+$ cells were predominantly concentrated in the intermediate zone (Fig. 5a), bore tangentially radiating multi-polar processes and expressed neuronal marker Tuj1 (Fig. 5b, d). Significantly fewer Tctex-1-sh-targeted cells displayed radial glia markers when compared with the controls (Fig. 5c, d), and almost none of them displayed Tbr2 (Supplementary Fig. S4d).

Second, to corroborate the cell-based phenotypic analysis *in situ*, the fraction of GFP$^+$ cells dissociated from the electroporated brains that also expressed Tuj1 was scored (Supplementary Fig. S4e). These results suggested that a significantly greater number of cells transfected with Tctex-1-sh were neurons. Third, quantitative reverse transcription PCR (RT–PCR) assays using RNAs isolated from flow cytometer-sorted GFP$^+$ cells showed that a significantly higher fraction of Tctex-1-silenced cells expressed Tuj1 in comparison with control cells (data not shown).

A neuron's birthdate is correlated with its laminar fate in the cortical plate as corticogenesis progresses; cells that differentiate at later time points tend to be found in the upper (more superficial) layers of the cortical plate[21]. In agreement with the proposed idea that Tctex-1-sh-targeted cells differentiate and migrate earlier, these cells were found to be located in a relatively deeper cortical layer, compared with the control cells in brains harvested 5 days after IUE (Fig. 5e, f). It was also noted that neurons derived from Tctex-1-sh-targeted cells, similarly to the controls, displayed neuronal markers (for example, HuD and doublecortin) and extended axons (data not shown). These results suggest that Tctex-1 expression is not critical for cell migration. Previous studies have shown that cytoplasmic dynein is important for cortical cell migration[22]. The differences in phenotype seen between the Tctex-1-suppressed and cytoplasmic-dynein-suppressed cells further support the idea that the role of Tctex-1 in corticogenesis is independent of its dynein-related activity.

Tctex-1 suppression drives radial glia exit from the cell cycle

We consistently observed that the total numbers of GFP$^+$ cells in brains transfected with Tctex-1-sh were fewer than those of the control brains (Fig. 5a). This discrepancy in cell number was not due to low transfection efficiency (Supplementary Fig. S5a, b) or apoptotic cell death (Supplementary Fig. S5c). Thus, the most probable explanation is that the Tctex-1-sh-transfected radial glia underwent a premature switch from proliferation to differentiation mode. Early depletion of the fast-proliferating progenitors could result in a detectably lower number of

total GFP$^+$ cells because the doubling times for E13–E14 radial glia are rather short (that is, 11.4–15.1 h) [3]. Indeed, compared with control cells, a significantly reduced fraction of Tctex-1-sh-transfected cells exhibited mitotic marker phosphohistone 3 (P-H3; Fig. 6a, c). The low mitotic index also precluded the possibility that Tctex-1-depletion caused mitotic arrest. Furthermore, as expected[23,24], the majority of ventricular zone mitotic cells transfected with vector alone had a vertical cleavage plane (that is, DNA in anaphase/metaphase cells are oriented 60°–90° relative to the axis of ventricle surfaces; Supplementary Fig. S5d). Among the few mitotic cells transfected with Tctex-1-sh, most of them also exhibited vertical cleavage. The difference in the fraction of cells displaying intermediate versus horizontal cleavages between Tctex-1-suppressed and control cells was also negligible.

To test how Tctex-1 knockdown affects cell cycling, we performed a cell cycle exit analysis *in situ*[25]. A single-pulse of BrdU was given to mice 24 h after IUE, and the brain slices harvested 24 h afterwards were immunolabelled for BrdU and Ki67. The fraction of GFP$^+$ BrdU$^+$ cells that were Ki67$^-$ (that is, cell-cycle-exit index) was found to be greater in cells transfected with Tctex-1-sh than in control cells (Fig. 6b, d).

All phenotypes elicited by Tctex-1 silencing—the distribution and number of transfected cells (Fig. 5a), the neuron-to-progenitor ratio (Fig. 5d), the mitotic indices (Fig. 6 c) and the cell-cycle-exit indices (Fig. 6d)—were successfully restored by both wild-type and Tctex-1^{T94E}, but not by Tctex-1^{T94A}. Taken together, these results suggest that phospho(T94)Tctex-1 is the active form of Tctex-1 in radial glia.

Phospho-mimic Tctex-1 accelerates S-phase entry and increases the proliferating progenitor population

If impaired ciliary disassembly caused by Tctex-1 silencing underlies the S-entry block of radial glia, the perturbation of a known inhibitor of cilium resorption should mimic the phenotypes exerted by Tctex-1-sh. Indeed, the majority of cells transfected with plasmids encoding *AurA* shRNA (AurA-sh) or *HDAC6* shRNA (HDAC6-sh) developed into intermediate-zone-residing neurons 40 h after electroporation (Fig. 7a), and displayed significantly lower mitotic indices (mitotic indices of AurA-sh and HDAC-6-sh transfected cells were 1% and 0.5%, respectively, versus 4.4% of control cells).

To carry out gain-of-function analysis, bicistronic vectors expressing both Tctex-1 (or its variants) and GFP were employed to perform IUE. We first showed that overexpression of Tctex-1^{T94E}, but not wild-type or Tctex-1^{T94A}, almost doubled the mitotic index in transfected neocortices (Fig. 7b, c). Furthermore, cell-cycle entry analysis, in which a single pulse of BrdU was given to the mice 2 h before harvest was carried out. The fraction of GFP$^+$ cells that were also BrdU$^+$ was significantly higher in cells transfected with Tctex-1^{T94E} than in those transfected with wild-type Tctex-1 or Tctex-1^{T94A} (Fig. 7d), suggesting that S-phase entry is accelerated in Tctex-1^{T94E}-overexpressing cells. Finally, we employed a cumulative BrdU labelling experiment to determine the cell cycle length of the radial glial cells[3]. The length of the G_2/M phase of Tctex-1^{T94E}-, GFP- and non-transfected progenitors was the same (2 h). However, the G_1 length of Tctex-1^{T94E}-transfected progenitors (6.8 h) was significantly shorter than that of untransfected or GFP-transfected progenitors (10 h; Fig. 7e). These results suggest that forced expression of phospho-mimic Tctex-1 expands the proliferating progenitor pool by shortening the G_1 phase and accelerating S-phase re-entry.

DISCUSSION

Human genetic studies have suggested a causal relationship between several ciliary/centrosomal proteins and the cellular overproliferation phenotype seen in cilium-related disorders, such as cystic kidney disease and certain brain development diseases[26]. However, the relationships between cilia, centrosomes and cell division are not well understood. Complete ciliary resorption before mitosis is thought to be necessary for the release of centrioles from basal bodies to form mitotic poles[18]. Several ciliated proteins have indeed been linked to the G_2/M transition and/or to cytokinesis[27,28]. The significance of ciliary shortening at late-G_1 phase and its relevance to the subsequent S-phase entry, however, is unknown. Here we present evidence that phospho(T94)Tctex-1 is required for cilium resorption, and hence S-phase entry.

Our data supports a model in which cilia provide a brake in the cell cycle to retain cells in G_0/G_1. Extracellular cues that activate the signalling pathways involved may determine the time required for this cellular event to take place and the duration of G_0/G_1. Cilia-mediated quiescence control may be absent in some non-ciliated cancerous cells[29]. These cells are thus likely to be insensitive to the environmental cues that time normal cells for division.

An understanding of the molecular switch between self-renewal and neuronal differentiation in cortical progenitors is critical in elucidating mechanisms that control brain size[30–32]. We speculate that radial glia receive ventricular cues via the cilium, allowing for subsequent recruitment of phospho(T94)Tctex-1 to guide timely ciliary resorption and proliferation. Blocking the activation of phospho(T94)Tctex-1 induces neuronal differentiation at the expense of proliferating progenitors, mimicking the developmental programme of late progenitors. Interestingly, several protein mutations found in human diseases associated with small brain size are localized to the centrosomes[33]. Although both previous[4,5,19,20] and our studies suggest G_1 length controls the cell fate determination of radial glia during corticogenesis, direct visualization and comparison of life cycle of radial glia with varying G_1 lengths remains to be shown.

The primary cilium is vital for the proper development of multiple brain regions. Sonic hedgehog signalling pathway transduced through cilia delivers a proliferative signal, which is required for the establishment and maintenance of neural progenitors of the cerebellum and hippocampus[34–36,37]. Thus, it seems that while the cilia are required to sense 'proliferation' signals, they are resorbed in a timely manner to permit the cells to re-enter the cell cycle. These two seemingly opposing roles of cilia could represent two temporally related events, working in conjunction to regulate cell division.

A link between the spindle orientation and the fate determination of mouse radial glia has been previously proposed[38], but remains controversial[23,24]. We did not observe any significant change in spindle orientation in Tctex-1 suppressed cells, suggesting that altering the cleavage plane was not a major contributor to the neural fate adoption of these cells. This finding differed from a previous report[39] where it was suggested that suppression of Tctex-1 expression has an impact on the spindle orientation of radial glia. Differences were noted between these two studies. First, different *Tctex-1* shRNA plasmids were used; we were able to rule out any off-target effect by performing *in vivo* rescue experiments. Second, we considered cells with cleavage plane at an angle greater than or equal to 30° oblique to the vertical plane to be anomalous[23,24,38]; the previous study considered 15° to be the reference point[39].

A recent report suggested that actin dynamics is involved in ciliogenesis[40]. Our data show that phospho(T94)Tctex-1-regulated ciliary resorption also occurs through a process involving actin cytoskeleton rearrangement. We envision that at the base of the cilium, Tctex-1 is dissociated from the dynein complex, through phosphorylation at Thr 94. Phosphorylated Tctex-1 activates local F-actin polymerization, which may trigger a cascade of cellular events that coordinately resorb the cilia and modify the basal bodies. The latter may transmit signals to programme the cells for S-phase entry, a mechanism that agrees with the finding that the centrosome/basal body is a central hub for almost all cell cycle-regulating proteins[41].

METHODS

Methods and any associated references are available in the online version of the paper at http://www.nature.com/naturecellbiology/

Note: Supplementary Information is available on the Nature Cell Biology website

ACKNOWLEDGEMENTS

We are indebted to the following grant support: Tri-Institutional Starr Foundation, NYSTEM, NIH (EY11307, EY016805), RPB (to C-H.S.), Tohoku University (to M.S.), New Energy and Industrial Technology Development Organization, and Grant-in-Aid for Scientific Research from the Ministry of Education, Science, Sports, and Culture of Japan (to K.T.). We thank G. Pazour, K. Anderson, R. Hevner, Y. Shi, N. Heintz, C. Cepko, A. Liu and S. Doxsey for reagents, and S. Anderson, M. E. Ross, D. Cobrinik and B. Tsou for discussion.

AUTHOR CONTRIBUTIONS

A.L., J-Z.C. and C-H.S designed the overall study. A.L. and C.D. performed IUE experiments and phenotype characterization. J-Z. C. generated all constructs. A. L., Y-Y.T. and M.S. performed cell culture studies. K.T. generated the anti-phospho(T94)Tctex-1 antibody. K.T. and T.K. generated 9R peptides. A.L., J-Z.C. and C-H.S. wrote the paper.

COMPETING FINANCIAL INTEREST STATEMENT

The authors declare that they have no competing financial interests.

Published online at http://www.nature.com/naturecellbiology
Reprints and permissions information is available online at http://npg.nature.com/reprintsandpermissions/

1. Pan, J. & Snell, W. The primary cilium: keeper of the key to cell division. *Cell* **129,** 1255–1257 (2007).
2. Alvarez-Buylla, A., Garcia-Verdugo, J. M. & Tramontin, A. D. A unified hypothesis on the lineage of neural stem cells. *Nat. Rev. Neurosci.* **2,** 287–293 (2001).
3. Takahashi, T., Nowakowski, R. S. & Caviness, V. S., Jr. The cell cycle of the pseudostratified ventricular epithelium of the embryonic murine cerebral wall. *J. Neurosci.* **15,** 6046–6057 (1995).
4. Lange, C., Huttner, W. B. & Calegari, F. Cdk4/cyclinD1 overexpression in neural stem cells shortens G1, delays neurogenesis, and promotes the generation and expansion of basal progenitors. *Cell Stem Cell* **5,** 320–331 (2009).
5. Pilaz, L. J. *et al.* Forced G1-phase reduction alters mode of division, neuron number, and laminar phenotype in the cerebral cortex. *Proc. Natl Acad. Sci. USA* **106,** 21924–21929 (2009).
6. Calegari, F. & Huttner, W. B. An inhibition of cyclin-dependent kinases that lengthens, but does not arrest, neuroepithelial cell cycle induces premature neurogenesis. *J. Cell Sci.* **116,** 4947–4955 (2003).
7. Pfister, K. K. *et al.* Cytoplasmic dynein nomenclature. *J. Cell Biol.* **171,** 411–413 (2005).
8. King, S. M. *et al.* The mouse *t*-complex-encoded protein Tctex-1 is a light chain of brain cytoplasmic dynein. *J. Biol. Chem.* **271,** 32281–32287 (1996).
9. Chuang, J. Z. *et al.* The dynein light chain Tctex-1 has a dynein-independent role in actin remodeling during neurite outgrowth. *Dev. Cell* **9,** 75–86 (2005).
10. Dedesma, C., Chuang, J. Z., Alfinito, P. D. & Sung, C. H. Dynein light chain Tctex-1 identifies neural progenitors in adult brain. *J. Comp. Neurol.* **496,** 773–786 (2006).
11. Pugacheva, E. N., Jablonski, S. A., Hartman, T. R., Henske, E. P. & Golemis, E. A. HEF1-dependent Aurora A activation induces disassembly of the primary cilium. *Cell* **129,** 1351–1363 (2007).
12. Mittnacht, S. Control of pRB phosphorylation. *Curr. Opin. Genet. Dev.* **8,** 21–27 (1998).
13. Follit, J. A., Tuft, R. A., Fogarty, K. E. & Pazour, G. J. The intraflagellar transport protein IFT20 is associated with the Golgi complex and is required for cilia assembly. *Mol. Biol. Cell* **17,** 3781–3792 (2006).
14. Jia, J. *et al.* Suppressor of Fused inhibits mammalian Hedgehog signaling in the absence of cilia. *Dev. Biol.* **330,** 452–460 (2009).
15. Murcia, N. S. *et al.* The Oak Ridge Polycystic Kidney (orpk) disease gene is required for left–right axis determination. *Development* **127,** 2347–2355 (2000).
16. Tucker, R. W., Pardee, A. B. & Fujiwara, K. Centriole ciliation is related to quiescence and DNA synthesis in 3T3 cells. *Cell* **17,** 527–535 (1979).
17. Schneider, L. *et al.* PDGFRαα signaling is regulated through the primary cilium in fibroblasts. *Curr. Biol.* **15,** 1861–1866 (2005).
18. Matsushita, M. *et al.* A high-efficiency protein transduction system demonstrating the role of PKA in long-lasting long-term potentiation. *J. Neurosci.* **21,** 6000–6007 (2001).
19. Dehay, C. & Kennedy, H. Cell-cycle control and cortical development. *Nat. Rev. Neurosci.* **8,** 438–450 (2007).
20. Gotz, M. & Huttner, W. B. The cell biology of neurogenesis. *Nat. Rev. Mol. Cell Biol.* **6,** 777–788 (2005).
21. Kriegstein, A. R. & Noctor, S. C. Patterns of neuronal migration in the embryonic cortex. *Trends Neurosci.* **27,** 392–399 (2004).
22. Shu, T. *et al.* Ndel1 operates in a common pathway with LIS1 and cytoplasmic dynein to regulate cortical neuronal positioning. *Neuron* **44,** 263–277 (2004).
23. Konno, D. *et al.* Neuroepithelial progenitors undergo LGN-dependent planar divisions to maintain self-renewability during mammalian neurogenesis. *Nat. Cell Biol.* **10,** 93–101 (2008).
24. Morin, X., Jaouen, F. & Durbec, P. Control of planar divisions by the G-protein regulator LGN maintains progenitors in the chick neuroepithelium. *Nat. Neurosci.* **10,** 1440–1448 (2007).
25. Chenn, A. & Walsh, C. A. Regulation of cerebral cortical size by control of cell cycle exit in neural precursors. *Science* **297,** 365–369 (2002).
26. Davenport, J. R. & Yoder, B. K. An incredible decade for the primary cilium: a look at a once-forgotten organelle. *Am. J. Physiol. Renal Physiol.* **289,** F1159–1169 (2005).
27. Mahjoub, M. R., Qasim Rasi, M. & Quarmby, L. M. A NIMA-related kinase, Fa2p, localizes to a novel site in the proximal cilia of *Chlamydomonas* and mouse kidney cells. *Mol. Biol. Cell* **15,** 5172–5186 (2004).
28. Qin, H., Wang, Z., Diener, D. & Rosenbaum, J. Intraflagellar transport protein 27 is a small G protein involved in cell-cycle control. *Curr. Biol.* **17,** 193–202 (2007).
29. Seeley, E. S., Carriere, C., Goetze, T., Longnecker, D. S. & Korc, M. Pancreatic cancer and precursor pancreatic intraepithelial neoplasia lesions are devoid of primary cilia. *Cancer Res.* **69,** 422–430 (2009).
30. Fish, J. L., Kosodo, Y., Enard, W., Paabo, S. & Huttner, W. B. Aspm specifically maintains symmetric proliferative divisions of neuroepithelial cells. *Proc. Natl Acad. Sci. USA* **103,** 10438–10443 (2006).
31. Higginbotham, H. R. & Gleeson, J. G. The centrosome in neuronal development. *Trends Neurosci.* **30,** 276–283 (2007).
32. Zhong, X., Pfeifer, G. P. & Xu, X. Microcephalin encodes a centrosomal protein. *Cell Cycle* **5,** 457–458 (2006).
33. Bond, J. & Woods, C. G. Cytoskeletal genes regulating brain size. *Curr. Opin. Cell Biol.* **18,** 95–101 (2006).
34. Chizhikov, V. V. *et al.* Cilia proteins control cerebellar morphogenesis by promoting expansion of the granule progenitor pool. *J. Neurosci.* **27,** 9780–9789 (2007).
35. Spassky, N. *et al.* Primary cilia are required for cerebellar development and Shh-dependent expansion of progenitor pool. *Dev. Biol.* **317,** 246–259 (2008).
36. Han, Y. G. *et al.* Hedgehog signaling and primary cilia are required for the formation of adult neural stem cells. *Nat. Neurosci.* **11,** 277–284 (2008).
37. Lai, K., Kaspar, B. K., Gage, F. H. & Schaffer, D. V. Sonic hedgehog regulates adult neural progenitor proliferation *in vitro* and *in vivo*. *Nat. Neurosci.* **6,** 21–27 (2003).
38. Chenn, A. & McConnell, S. K. Cleavage orientation and the asymmetric inheritance of Notch1 immunoreactivity in mammalian neurogenesis. *Cell* **82,** 631–641 (1995).
39. Gauthier-Fisher, A. *et al.* Lfc and Tctex-1 regulate the genesis of neurons from cortical precursor cells. *Nat. Neurosci.* **12,** 735–744 (2009).
40. Kim, J. *et al.* Functional genomic screen for modulators of ciliogenesis and cilium length. *Nature* **464,** 1048–1051 (2010).
41. Doxsey, S., Zimmerman, W. & Mikule, K. Centrosome control of the cell cycle. *Trends Cell Biol.* **15,** 303–311 (2005).
42. Caspary, T., Larkins, C. E. & Anderson, K. V. The graded response to Sonic Hedgehog depends on cilia architecture. *Dev. Cell* **12,** 767–778 (2007).
43. Takeuchi, A. & O'Leary, D. D. Radial migration of superficial layer cortical neurons controlled by novel Ig cell adhesion molecule MDGA1. *J. Neurosci.* **26,** 4460–4464 (2006).

METHODS

Cell cultures, transfection and cilium assembly/disassembly assay. IFT20KD-RPE-1 was a gift from G. Pazour[13] (University of Massachussets Medical School; USA). Immortalized wild-type MEF and *Ift88* mutant MEF cells were gifts from A. Liu[14] (Pennsylvania State University, USA). MEF, RPE-1 and 3T3 cells were transfected using nucleofection (Amaxa). HeLa cells were transfected using Lipofectamine 2000 (Invitrogen). COS-7 and HEK cells were transfected using the polyethylenimine method[44]. Protein expression levels were estimated by immunoblotting and quantified by Odyssey Infrared scanner (LI-COR). For most immunolabelling, cultured cells were fixed in 4% paraformaldehyde for 10 min and then submerged in cold methanol for 5 min before the blocking and antibody incubation using standard procedures.

A cilium assembly/disassembly assay was performed as previously described[11]. Specifically, cells were starved in serum-free medium for 48 h to induce cilium formation. Serum was then added back to the medium to stimulate cilium resorption and cell cycle re-entry. Cells were harvested at various time points for immunolabelling assays. All plasmids used for overexpression experiments in cultures were under the CMV promoter. Cells receiving more than one plasmid were routinely immunolabelled to confirm high (> 90%) double or triple transfection efficiency.

Purified recombinant proteins (for example, GFP-9R, Tctex-$1^{T94E\text{-}9R}$ and Tctex-$1^{T94A\text{-}9R}$; 1 μM) were added into cilium-preformed cells in the absence of serum for 30 min[18]. Cells were then gently rinsed and transferred to peptide-free, serum-free medium for different time periods before fixation. In some experiments, Cyto D (0.5 μM, Sigma) was included in the medium 1 h before the peptide addition and thereafter.

BrdU incorporation index. For the experiments carried out in synchronized cells, 12-hr post-transfected cells were induced to growth arrest by 48 h serum starvation. Cells were then cultured in regular medium for 12 hr, pulse labelled with 1 hr BrdU (10 μM), and followed by a 12 hr chase. These cells were subsequently treated with acid followed by BrdU labelling. The fractions of GFP^+ transfected cells with BrdU incorporated were counted, and the BrdU incorporation indices were shown by considering the control as 100%. For the experiments carried out in unsynchronized cells, cells 48 hr post-transfection wee treated with BrdU for 12 hr, followed by GFP and BrdU labelling. For the protein transduction experiments, BrdU was added into serum-free medium for 12hr immediately after the 30-min incubation of peptides.

IUE, immunohistochemistry of mouse brain slices, and quantitative analyses. IUE procedures were performed on E13.5 CD1 mouse brains using plasmids driven by either CAG or U6 promoter, as described[45]. At specific time points, electroporated brains were harvested, fixed with 4% paraformaldehyde overnight at 4°C, embedded in low melting agarose, and sectioned by vibratome. Sectioned brain slices were subsequently subjected to immunostaining. For the ventricle surfaces of E11–E17 neocortical slices, triple-labelled for Arl13b, Tctex-1 phosphorylated at Thr 94 and γ-tubulin, cortical slices were first incubated with antibody against Tctex-1 phosphorylated at Thr 94, followed by excess biotinylated goat-anti-rabbit antibody. The sections were then PFA fixed, incubated with anti-Arl13b and γ-tubulin antibodies, followed by detection by using Alexa488-conjugated anti-rabbit, Cy5-conjugated anti-mouse antibody, and Alexa568-conjugated streptavidin. All immunolabelled sections were analysed by Leica TCS SP2 spectral confocal system (Nussloch, Germany), as previously described[10]. In some experiments, electroporated brains were dissociated with papain (Worthington) and dispersed on poly-L-lysine coated coverslips. After a 2-h 37°C incubation, cells were fixed with 4% paraformaldehyde followed by immunostaining. All animal manipulations were performed in accordance with the guidelines for animal experiments at Weill Medical Cornell IACUC.

Mitotic index, cell-cycle exit and cell-cycling analyses in brain slices. The mitotic index of treated brain slices was determined as the ratios of GFP^+ and $P\text{-}H3^+$ cells to the total GFP^+ transfected cells in the ventricular zone/subventricular zone. Cell cycle analysis was performed as described[46]. Briefly, pregnant mice were injected with BrdU (50 mg per kg body weight) 24 h after IUE, and fetal brains were harvested 24 h after BrdU treatment. Brain slices were then immunolabelled for GFP, BrdU and Ki67. The cell-cycle-exit index of GFP-transfected cells was determined as a ratio of the GFP-labelled cells that exited the cell cycle (GFP^+, $BrdU^+$ and $Ki67^-$) to total GFP-labelled cells with BrdU incorporation (GFP^+ and $BrdU^+$). For S-phase entry analysis, IUE-treated animals were treated with BrdU (50 mg per kg body weight) for 2 h before harvest. In all cases, similar areas in the transfected neocortices were selected for analysis. Calculation of cell cycle phases was carried out using cumulative BrdU incorporation, as described[3]. Briefly, BrdU injection started at E14.5 (24 h post-electroporation) and continued at 3-h intervals. Mice were sacrificed 2, 3, 6, 9 or 12 h after the first BrdU injection. 100% BrdU incorporation refers to when all ventricular zone cells are labelled with BrdU. The length of G_2/M was taken to be the time required to label all mitotic cells, based on chromatin condensation. The length of G_1 was estimated as described[3].

Production and specificity verification of phospho-specific antibodies for Tctex-1. Rabbits were injected with a peptide (TDGSC(pT)VRWEN) corresponding to amino-acid positions 89–99 of human Tctex-1 with chemical phosphorylation on the Thr 94 residue. The resulting serum was affinity purified with a phospho-peptide column. The affinity-purified antibody specifically detected the phosphorylated peptide but not the unphosphorylated peptide in an ELISA (enzyme-linked immunosorbent assay).

Reagents. Two human *Tctex-1*-siRNA oligonucleotides (targeting sequence: 5′-GAGGCTAUAGAAAGCGCAATT-3′ and 5′-TACATCGTGACCTGTGTAATT-3′) and a mouse Tctex-1-siRNA (targeting sequence: 5′-GTCAACCAGTGGACCACT-3′) were synthesized by Thermo Fisher (Waltham). Both control-siRNA and AurA-siRNA oligonucleotide were purchased from Santa Cruz Biotech (Santa Cruz). To generate short-hairpin encoding plasmid, the annealed targeting-oligonucleotides were first inserted into pU6-promoter-driven vector (gift of Y. Shi, Harvard University, USA), as suggested[47]. The entire shRNA expression cassette was then transferred into pCAG-IRES-GFP vector (gift from C. Cepko, Harvard University, USA); the resulting construct thus also encoded GFP under the CAG promoter. The targeting sequences for mouse and human *Tctex-1* shRNA were 5′-GGGTTACACTCCGCAAGTTCC-3′ and 5′-GGGACAGCTCTACTGACGGGA-3′, respectively. The targeting sequence for (mouse and human) *HDAC6* shRNA was 5′-GGGTTATGCCCACCTCACCCAC-3′. Three control shRNA plasmids were used; one was purchased from Applied Biosystem (Austin, TX) and two were synthesized (the targeting sequences were 5′-GGGATCGTAGGTTCTCGAAA-3′ and 5′-GGGCTATACCAAGAGACATGC-3′). For ectopic expression *in vivo*, cDNA fragments encoding Tctex-1 (e.g.,wild-type, Tctex-1^{T94E} or Tctex-1^{T94A}; ref. 9) were cloned into either pCAG-IRES-GFP or Tctex-1-sh/GFP plasmid. pRK5 vector encoding wild-type, Tctex-1^{T94E}, and Tctex-1^{T94E}, described in ref.9, were used to perform the *in vitro* expression. GFP-9R and Tctex-1-9R were generated in pET21a vector (Novagen), and recombinant proteins were expressed in BL21 (DE3) cells and purified by Ni-NTA agarose column (Invitrogen)[18].

The primary antibodies used were: acetylated α-tubulin mouse immmunoglobulin G2b (IgG_{2b}; 1:400, Sigma), Arl13b rabbit antibody (1:500, gift from K. Anderson[42], Memorial-Sloan Kettering Cancer Center, USA), α-tubulin mouse antibody (1:1,000, GE Health), brain lipid-binding protein rabbit antibody (1:2,500, gift from N. Heintz[48], Rockefeller University, USA), BrdU rat antibody (1:200, Harlan), active caspase 3 rabbit antibody (1:200, Abcam), dynein intermediate chain mouse antibody (1:10,000, Millipore), Flag mouse and rabbit antibodies (1:500, Sigma), GFP rabbit antibody (1:1,000, Invitrogen), GFP chicken antibody (1:2,000, Abcam), GFP mouse antibody (1: 1,000, Millipore), γ-tubulin mouse antibody (clone GTU-88, immunoglobulin G1, IgG_1; 1: 2,000, Sigma), Ki67 rabbit antibody (1:500, Novocastra), Nestin mouse antibody (clone 401, 1: 200, Developmental Studies Hybridoma Bank), P-H3 rabbit antibody (1:200, Millipore), Tbr2 rabbit antibody (1:1,000, gift from R. Hevner[49], University of Washington School of Medicine, USA), protein A-purified Tctex-1 mouse antibody (1:1,000, this paper), affinity-purified Tctex-1 rabbit antibody[50] (1:100), Tuj1 mouse antibody (1:500, Covance), ZO-1 mouse antibody (1:500, Invitrogen), phospho-Rb (Ser795), phospho-Rb(Ser807/811), and phospho-cdc2 (Tyr15) rabbit antibodies (1:1,000, Cell Signalling Technology). Alexa-conjugated streptavidin or secondary antibodies (anti-mouse, anti-rabbit, anti-rat, anti-IgG_{2b}; 1:400) were purchased from Invitrogen; biotinylated anti-IgG_1 and Cy5-conjugated streptavidin were purchased from Jackson Lab (used at 1:200; West Grove). In this study, negative controls involved omission of the primary antibody and use of antibody that had been pre-absorbed with antigen. Co-labelling of acetylated α-tubulin (mouse IgG_{2b}) and γ-tubulin (mouse IgG_1) in this study involved using isotype-specific mouse immunoglobulins.

DOI: 10.1038/ncb2218

Microscopic and statistical analyses. All the quantification studies were carried out in transfected cells localized within the dorsolateral neocortex to avoid possible variation within particular brain regions. At least three independent brains were analysed for each DNA construct. Analysis of the immunostained sections was carried out on a Leica TCS SP2 spectral confocal system. To improve observer objectivity, image capture and analysis were done at separate times in a double-blind fashion. To score images, the GFP channel was first judged independently, followed by judgments of the other markers. For Ki67 and BrdU-nuclear labelling, small puncta or signals that were not compliant with the DAPI (4,6-diamidino-2-phenylindole) nuclear labelling were ignored.

Statistical analysis was performed with GraphPad software (GraphPad Prism v4.0, GraphPad Software). Data are presented as the mean ± s.e.m. from at least three representative independent experiments. *t*-test was designed for the comparison of two groups. One-way analysis of variance (ANOVA) was applied for the comparisons in which only one independent variable was being analysed. The Dunnet test (as a *post hoc* test) was used to compare data samples versus control. Statistical significance was defined as $P < 0.05$, 0.01 or 0.001.

44. Thomas, M. *et al.* Full deacylation of polyethylenimine dramatically boosts its gene delivery efficiency and specificity to mouse lung. *Proc. Natl Acad. Sci. USA* **102,** 5679–5684 (2005).
45. Tabata, H. & Nakajima, K. Efficient *in utero* gene transfer system to the developing mouse brain using electroporation: visualization of neuronal migration in the developing cortex. *Neuroscience* **103,** 865–872 (2001).
46. Sanada, K. & Tsai, L. H. G protein βγ subunits and AGS3 control spindle orientation and asymmetric cell fate of cerebral cortical progenitors. *Cell* **122,** 119–131 (2005).
47. Xia, X. G. *et al.* An enhanced U6 promoter for synthesis of short hairpin RNA. *Nucleic Acids Res.* **31,** e100 (2003).
48. Feng, L., Hatten, M. E. & Heintz, N. Brain lipid-binding protein (BLBP): a novel signaling system in the developing mammalian CNS. *Neuron* **12,** 895–908 (1994).
49. Hevner, R. F. *et al.* Tbr1 regulates differentiation of the preplate and layer 6. *Neuron* **29,** 353–366 (2001).
50. Tai, A. W., Chuang, J.-Z. & Sung, C.-H. Localization of Tctex-1, a cytoplasmic dynein light chain, to the Golgi apparatus and evidence for dynein complex heterogeneity. *J. Biol. Chem.* **273,** 19639–19649 (1998).

nature
cell biology

DOI: 10.1038/ncb2218

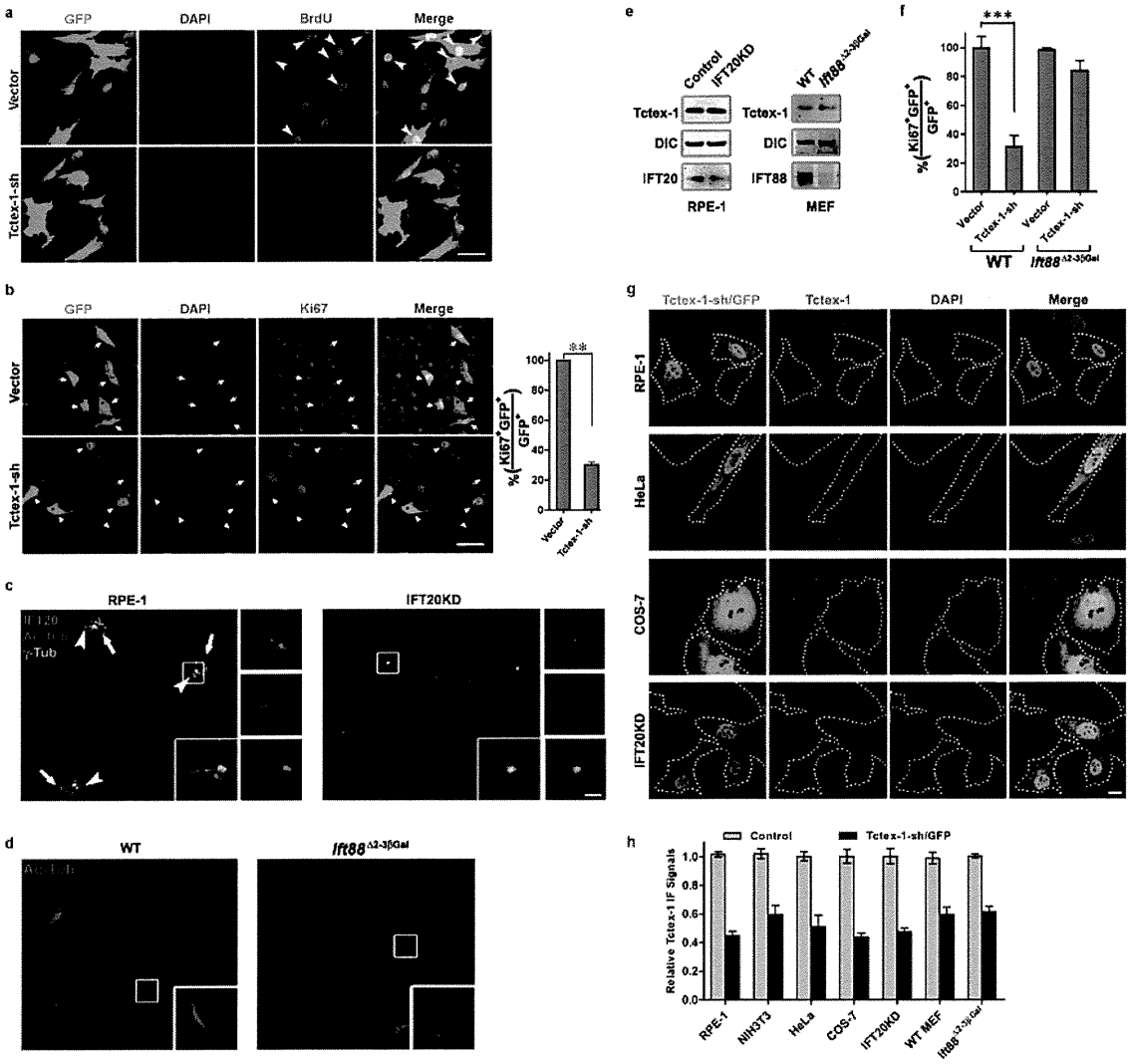

Figure S1 (**a**) BrdU labeling of RPE-1 cells transfected with vector or Tctex-1-sh. Arrowheads point to cells double positive for GFP and BrdU. (**b**) (Left) Ki67 labeling of RPE-1 cells transfected with vector or Tctex-1-sh. Arrows point to cells double positive for Ki67 and GFP; arrowheads point to the cells positive for GFP and negative for Ki67. (Right) Quantification of the percentage of $Ki67^{+}GFP^{+}$ cells out of total GFP^{+} cells (mean±s.e.m.; n=3 experiments; **p<0.01, *t*-test). (**c**) Immunolabeling of serum-starved RPE-1 and IFT20KD-RPE-1 cells for IFT20 (green), acetylated a-tubulin (red), and g-tubulin (cyan). These results showed that, consistent with the previous report, the endogenous IFT20 immunoreactivity was enriched at the Golgi apparatus in the parental RPE-1 cells (arrows), but diminished in the IFT20KD-RPE-1 cells. Enlarged boxed areas showed that the primary cilia (arrowheads) were readily detectable in RPE-1 cells, but not in IFT20KD-RPE-1 cells. Cytoplasmic acetylated a-tubulin labeling remains, however, detectable in the latter. (**d**) Acetylated a-tubulin immunolabeling verified the presenceand absence of primary cilia in WT and *Ift88* mutant MEF cells, respectively. (**e**) Immunoblots showed specific reduction of endogenous IFT20 in IFT20-KD RPE cells and specific depletion of IFT88 in *Ift88* mutant MEF cells. The levels of Tctex-1 and DIC were not affected in these cells. (**f**) Fractions of Ki67-labeled cells in GFP^{+} transfected cells are shown (mean ± s.e.m.; n=3 experiments; ***p<0.001, *t*-test). (**g**) Representative images show endogenous Tctex-1 immunofluorescence (red) were specifically reduced in cells transfected with Tctex-1-sh/GFP plasmids. Dotted lines depict the cell borders. (**h**). Quantification of Tctex-1 immunofluorescence between untransfected (control) and Tctex-1-sh transfected cells. An average of 20 cells were scored for each group. Bars= 50 mm (a, b), 2 mm (c), 10mm (g).

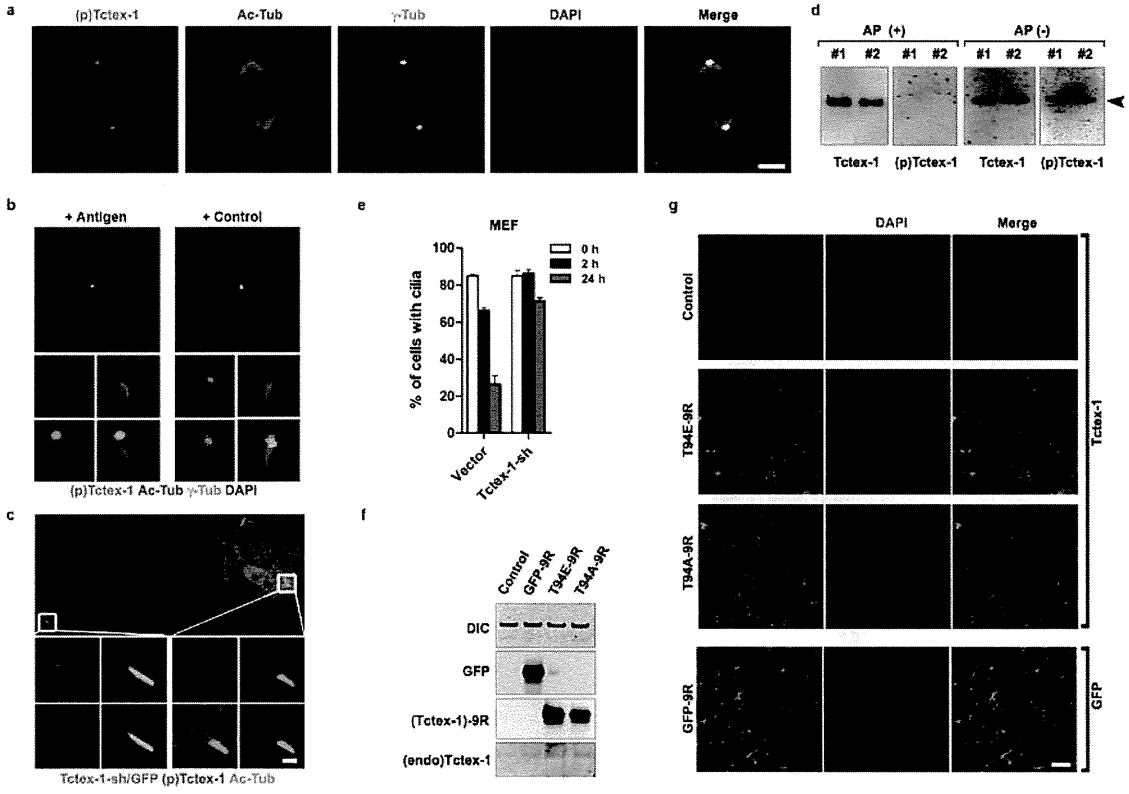

Figure S2 (**a**) 24-hr post-serum RPE-1 cells immunolabeled for phosph(T94)Tctex-1 (green), acetylate-a-tubulin (red), and g-tubulin (cyan). Bar=5 mm. (**b**) 2-hr post-serum RPE-1 RPE-1 cells were labeled with Ab recognizing phospho(T94)Tctex-1 (green) that was preabsorbed with phosphopeptides corresponding to the antigen (left) or control non-phosphopeptides (right). Acetylated a-tubulin (red) and g-tubulin (cyan) were also co-labeled. (**c**) Immunolabeling of 2-hr postserum RPE-1 cells showed that phospho(T94)Tctex-1 was present at the ciliary bases of untransfected cells, but was absent from the GFP+, Tctex-1-sh plasmid transfected cells. Bar= 2 mm. (**d**) Protein blots containing two independent duplicates (#1 and #2) of RPE-1 cell lysates harvested at 24-hr post-serum time points. These blots were either treated (+) or not treated (-) by alkaline phosphatase (AP), and followed by Tctex-1 or phospho(T94)Tctex-1 Ab probing. (**e**) Disassembly of cilia in MEF cells transfected with control vector or Tctex-1-sh plasmid. The fractions of transfected cells containing a cilium harvested at various time points after serum addition are shown (mean ± s.e.m.; n=3 experiments). (**f**) Immunoblotting assays demonstrated the highly efficient and roughly equivalent uptake of various 9R-peptides. Tctex-1-9R migrated slightly slower than did endogenous (endo) Tctex-1 due to the positive charges of the arginine residues. Mock treated cells were used as controls. (**g**) Immunolabeling of Tctex-1 or GFP for cells transduced with various peptides.

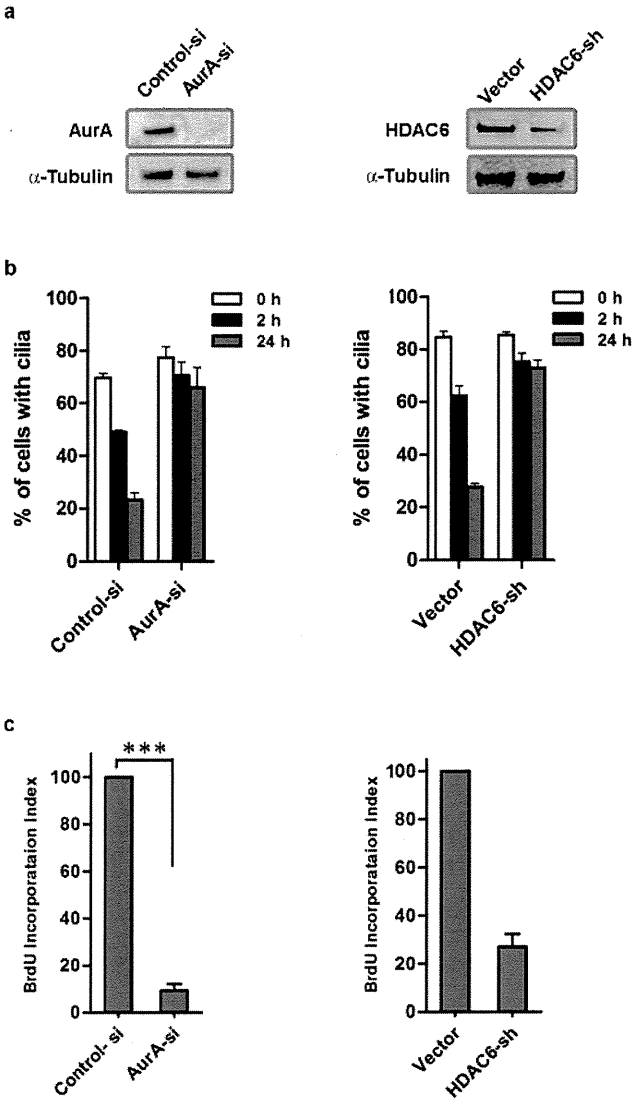

Figure S3 Immunoblotting **(a),** cilium disassembly (**b**), and BrdU incorporation (**c**) assays of RPE-1 cells transfected with either AurA-si or HDAC6-sh versus controls. All data shown were means ± s.e.m. (n=3 experiments; ***p<0.001, *t*-test).

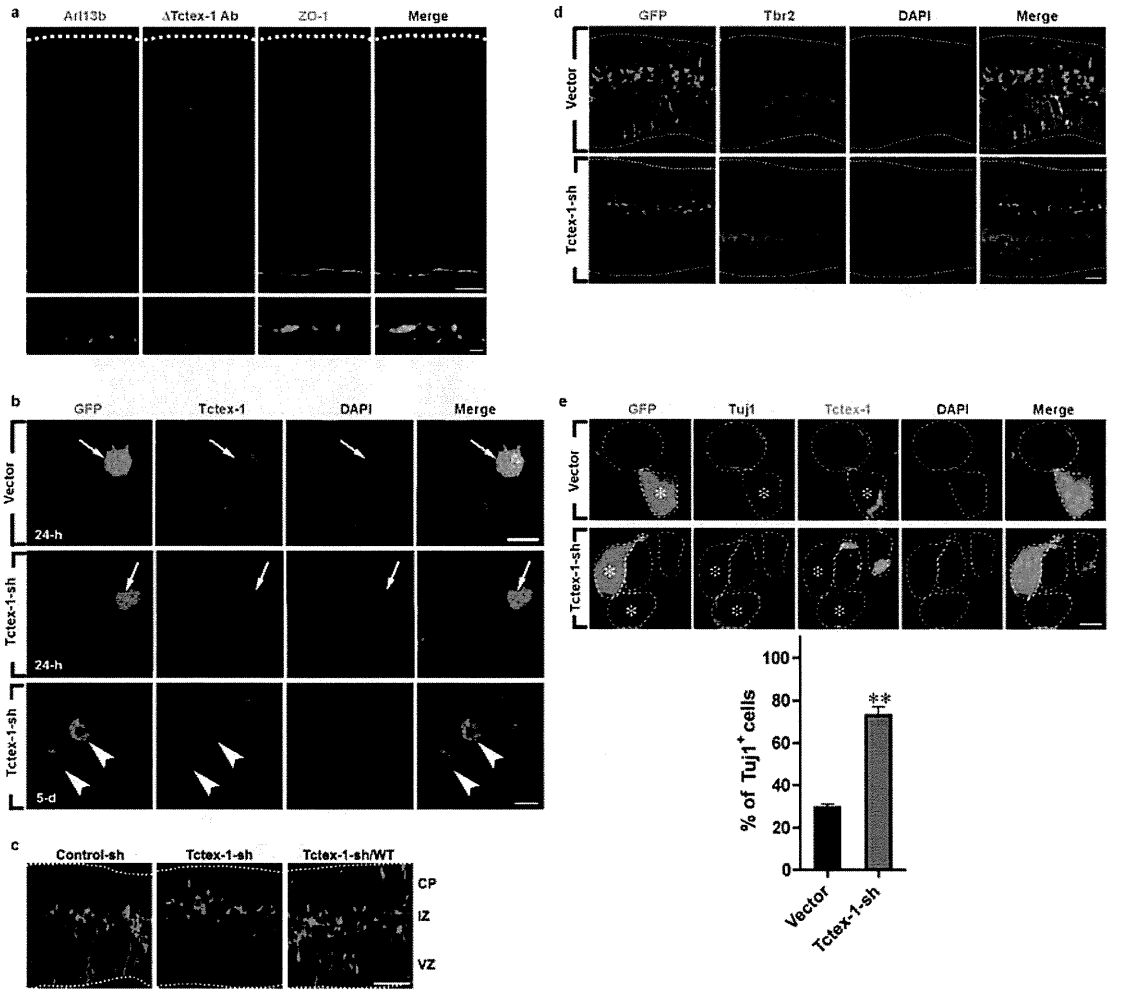

Figure S4 (a) Negative control for the confocal image shown in Fig. 4b by omitting (D) the primary Ab against Tctex-1. Bars= 20 mm (top panel); 2 mm (bottom panel). (**b**) Tctex-1 immunolabeling of cells dissociated from brains electroporated with control vector or Tctex-1-sh 24 hr or 5 days after electroporation. Arrows and arrowheads point to the transfected GFP+ cells harvested at 24-hr and 5-day time points, respectively. (**c**) Brain slices transfected with control-sh, Tctex-1-sh, and Tctex-1-sh/WT plasmids. (**d**) Tbr2 labeling of cortical slices transfected with GFP or Tctex-1-sh plasmid. (**e**) Cells dissociated from brains harvested 40 hr after electroporation were acutely fixed and immunolabeled for Tuj1. Asterisks mark transfected GFP+ cells; dotted lines mark the cell borders. Control transfected cells had a normal level of Tctex-1, and they are often negative for Tuj1. The quantification results show the percentage of GFP+ cells that were also Tuj1 (means ± s.e.m.; n=3 experiments; total of 350 GFP+ cells were scored; **p<0.01 (*t*-test). Bars= 10 mm (a-b, d); 50 mm (c).